Pion photoproduction in chiral perturbation theory with explicit treatment of the Δ(1232) resonance

N. Rijneveen,[1,*] A. M. Gasparyan,[1,2,†] H. Krebs,[1,‡] and E. Epelbaum[1,§]

[1]*Ruhr-Universität Bochum, Fakultät für Physik und Astronomie, Institut für Theoretische Physik II, D-44780 Bochum, Germany*

[2]*NRC Kurchatov Institute-ITEP, B. Cheremushkinskaya 25, 117218 Moscow, Russia*

(Received 19 August 2021; accepted 21 July 2022; published 22 August 2022)

We study the reaction of pion photoproduction on the nucleon in the framework of chiral perturbation theory with explicit Δ(1232) degrees of freedom. In the covariant approach, we give results up to order ϵ^3 in the small scale expansion scheme. Furthermore, we provide Δ-less and Δ-full results obtained in the heavy-baryon scheme to analyze the differences from the covariant approach. Low-energy constants are fitted to multipole amplitudes using theoretical truncation errors estimated by a Bayesian approach. We also compare our findings to data of neutral pion production cross sections and polarization asymmetries. The description of the reaction is clearly improved by the explicit treatment of the Δ(1232) resonance.

DOI: 10.1103/PhysRevC.106.025202

I. INTRODUCTION

In this work, we study the process of pion photoproduction on the nucleon, i.e., $\gamma + N \to \pi + N$, in the framework of chiral perturbation theory (χPT) with explicit Δ degrees of freedom. Studying this reaction is motivated by several reasons. First, it is the photoproduction of the lightest hadron. From the theoretical point of view, it is one of the simplest processes involving three different particles, and it thus serves as a test field for more complex reactions. From the experimental point of view, this reaction is quite easily accessible close to threshold and there can be no other hadronic final states due to energy conservation. Therefore, a lot of experimental data on pion photoproduction are available. As an additional motivation, pion photoproduction contributes as a subprocess to more complicated reactions, e.g., in radiative pion photoproduction, $\gamma + N \to \gamma + \pi + N$, providing an access to the magnetic moment of the Δ resonance [1], or in the interaction of nuclei with electromagnetic probes [2–7].

Pion photoproduction has been a research topic for many years, with the first model-independent approach proposed by Kroll and Ruderman in the 1950s [8]. Based on general principles, such as Lorentz and gauge invariance, they derived a low-energy theorem for the matrix element of charged pion photoproduction at threshold, which expressed the production amplitudes in terms of a series in the parameter $\mu = M_\pi/m_N$, where M_π and m_N refer to pion and nucleon masses, respectively. Later on, these predictions were improved [9,10] by including the so-called partially conserved axial-vector current hypothesis [11–13] and current algebra [14–16]. Until the 1980s, there was little doubt about the validity of the low-energy predictions. Particularly for the charged production channels, which are dominated by the Kroll-Ruderman term, the results from the theorem matched the available data well. However, new data for the neutral production channel at threshold [17,18] showed a non-negligible disagreement with the theoretical predictions for the *s*-wave electric dipole amplitude E_{0+}. A first important success for χPT was the study by Bernard, Kaiser, Gasser, and Meißner [19,20] on pion photoproduction, which corrected the low-energy theorems by terms arising from pion loop diagrams. However, these corrections, generated by infrared singularities of the loop integrals even worsened the agreement with data, which is due to the slow convergence of the chiral expansion in the neutral pion production channel. Therefore, renewed interest in pion photoproduction was awakened in the following years, and multiple experimental groups remeasured pion photo- and electroproduction reactions (see, e.g., Refs. [21–40]). In parallel, Bernard *et al.* worked out all the theoretical details in the different reaction channels within the framework of heavy-baryon chiral perturbation theory (HBχPT) [20,41–49]. An improvement of the convergence of the chiral expansion has been achieved by extending the pure χPT approach by means of dispersion-relation techniques [50].

The new approaches of the so-called infrared renormalization [51] and the extended-on-mass-shell (EOMS) scheme [52] enabled the treatment of scattering processes in the pion-nucleon sector in a manifestly covariant framework. Consequently, covariant calculations of $\gamma + N \to \pi + N$ were completed up to the leading loop order $\mathcal{O}(Q^3)$ in Ref. [53] using the infrared renormalization scheme, followed by an analysis of the full one-loop order $\mathcal{O}(Q^4)$ by Hilt *et al.* [54,55] in the EOMS scheme.

After it was worked out how to include the Δ resonance as an explicit degree of freedom into χPT within the so-called small scale expansion (SSE) scheme [56,57], the

*nora.rijneveen@rub.de
†ashot.gasparyan@rub.de
‡hermann.krebs@rub.de
§evgeny.epelbaum@rub.de

photoproduction of pions has also been considered in this extended framework. An explicit treatment of the Δ is of great interest, because the small gap between the pion production threshold and the Δ mass suggests that effects of the Δ may become important close above threshold. For example, the M_{1+} multipole receives dominant effects from the Δ resonance for energies close to the Δ mass. In SSE, the Δ-nucleon mass splitting $\Delta \equiv m_\Delta - m_N$ is considered to be of the same order as the pion mass, i.e., $\Delta \sim M_\pi \sim \epsilon$. The first calculation of pion photoproduction with explicit Δ degrees of freedom was completed in HBχPT [56], focusing on the neutral production channel close to threshold, which showed only moderate effects of the explicit Δ treatment. A subsequent HBχPT study [58] found a more distinct improvement of the description in the HB framework. In the covariant approach, studies of pion photoproduction at threshold were done in Refs. [59–62], finding a substantial improvement in the description of the data compared to the HB approach with explicit Δ's. However, in these works a different power counting [63] is used, the so-called δ scheme, in which the Δ-nucleon mass splitting Δ is considered to be of one order lower than the pion mass: $\Delta \sim \delta$, $M_\pi \sim \delta^2$. The motivation for such a counting is given by numerical arguments. Since there is no clear evidence for a faster convergence or better efficiency of one of the two schemes, it is desirable to consider pion photoproduction in the SSE for comparison purposes. Note, however, that the low-energy constants (LECs) of the two approaches cannot be compared directly, because their numerical values are scheme dependent. Comparing the results in two counting schemes can be done only in terms of quality of the data description.

We study pion photoproduction in both heavy-baryon and covariant formalisms of chiral effective field theory. We also analyze the effects of explicit Δ degrees of freedom by taking into account their leading-order and next-to-leading-order contributions in the covariant formalism of χPT within the EOMS scheme. To estimate theoretical uncertainties of observables and LECs, we use a Bayesian model [64–66].

First, we study the Δ-less case up to order Q^3, which has been considered before [53–55]. Recent studies were mainly focused on the covariant approach, so we provide a detailed comparison of the two formalisms in order to analyze the difference in convergence and data description. In particular, we compare the obtained LECs in terms of the effects generated by the infrared regular (IR) parts of the integrals. The extraction of the heavy-baryon LECs is very important for use in few-body applications such as calculation of the nuclear electroweak currents. That is why we choose to work in the so-called NN counting used in the few-nucleon calculations, although it can make the heavy-baryon expansion in pion photoproduction even less efficient.

Next, we upgrade the covariant calculation to leading-order Δ tree contributions employing the SSE, which has been used for studies of other reactions such as pion-nucleon scattering and Compton scattering (see, e.g., Refs. [67–69]). We also discuss the differences to the Δ-less case in terms of resonance saturation. Moreover, we provide results for the reaction $\gamma + N \to \pi + N$ up to leading Δ-full loop order for the first time. In comparison to the study of Ref. [60], we take into account loop diagrams including up to three Δ propagators, which give rise to significant contributions to the amplitude while maintaining gauge invariance. Furthermore, we give an estimate for the subleading $\gamma N\Delta$ coupling constant h_1. A qualitative comparison to the aforementioned studies in the δ scheme is given. Furthermore, we compare some of our results to recent high-precision data in the neutral pion production channel [38,39,70].

Our paper is structured as follows. In Sec. II, we introduce the basic formalism, such as kinematics, isospin and spin decomposition of the matrix elements, and calculation of multipole amplitudes and observables. In Sec. III, we list all terms of the effective Lagrangian relevant for our calculation and discuss the employed power-counting scheme. Subsequently, we discuss renormalization in Sec. IV. We present our results in Sec. V and conclude with a short summary in Sec. VI.

II. FORMALISM

In this section, we briefly introduce our notation for kinematics, isospin and spin decomposition, as well as the calculation of multipole amplitudes and observables. Pion photoproduction,

$$\gamma(\lambda, k) + N_i(s, p) \to \pi_c(q) + N_j(s', p'), \tag{1}$$

is a reaction where a pion is produced by absorption of a photon from a nucleon. Here, p (p'), s (s'), and i (j) are momentum, helicity, and isospin index of the incoming (outgoing) nucleon, k and λ are momentum and helicity of the photon, and q and c are momentum and isospin index of the pion, respectively. The kinematics of the reaction is uniquely defined by two Lorentz-invariant Mandelstam variables:

$$s = (p+k)^2 = (p'+q)^2, \quad t = (p-p')^2 = (k-q)^2. \tag{2}$$

The energies of the photon ω and the pion E_π in the center-of-mass (c.m.) frame expressed in terms of the Mandelstam variables read

$$\omega = \frac{s - m_N^2}{2\sqrt{s}}, \quad E_\pi = \frac{s + M_\pi^2 - m_N^2}{2\sqrt{s}}. \tag{3}$$

In the laboratory frame, the photon energy can be calculated from the total c.m. energy using

$$\omega_{\text{lab}} = \frac{s - m_N^2}{2m_N}. \tag{4}$$

Furthermore, we define the scattering angle θ via $|\boldsymbol{k}|\,|\boldsymbol{q}|\cos(\theta) = \boldsymbol{k}\cdot\boldsymbol{q}$, such that

$$t = M_\pi^2 - 2(\omega E_\pi - |\boldsymbol{k}|\,|\boldsymbol{q}|\cos(\theta)). \tag{5}$$

The pion production threshold lies at the c.m. energy of $\sqrt{s} = m_N + M_\pi$. In the HB formalism, an explicit $1/m_N$ expansion of the amplitude is performed. Expanding Eq. (3) in terms of $1/m_N$, we can derive an approximate relation between photon and pion c.m. energy:

$$\omega = E_\pi - \frac{M_\pi^2}{2m_N} + \mathcal{O}\left(\frac{1}{m_N^2}\right). \tag{6}$$

Thus, in the HB formalism, we express all kinematic quantities in terms of the pion energy E_π.

In the isospin space, the matrix elements of pion photoproduction can be parametrized in terms of three independent structures,

$$T^c_{\gamma N\to\pi N} = \delta_{c3}\, T^{(+)}_{\gamma N} + \tau_c\, T^{(0)}_{\gamma N} + \mathrm{i}\varepsilon_{c3a}\,\tau_a\, T^{(-)}_{\gamma N}, \tag{7}$$

where τ^i are the Pauli matrices in the isospin space. In Eq. (7), T can refer to the pion photoproduction amplitude in any representation including the photoproduction multipoles.

The matrix elements for the four physical pion photoproduction reaction channels

$$\gamma p\to\pi^0 p, \quad \gamma p\to\pi^+ n, \quad \gamma n\to\pi^0 n, \quad \gamma n\to\pi^- p, \tag{8}$$

can be obtained from the three isospin structures by using the following relations:

$$\begin{aligned} T_{\gamma p\to\pi^0 p} &= T^{(+)}_{\gamma N} + T^{(0)}_{\gamma N}, & T_{\gamma p\to\pi^+ n} &= \sqrt{2}\big(T^{(0)}_{\gamma N} + T^{(-)}_{\gamma N}\big),\\ T_{\gamma n\to\pi^0 n} &= T^{(+)}_{\gamma N} - T^{(0)}_{\gamma N}, & T_{\gamma n\to\pi^- p} &= \sqrt{2}\big(T^{(0)}_{\gamma N} - T^{(-)}_{\gamma N}\big). \end{aligned} \tag{9}$$

Another commonly used decomposition of the pion photoproduction amplitude is the so-called isospin parametrization in terms of the three amplitudes $T^{(\frac{3}{2})}_{\gamma N}$, $T^{(\frac{1}{2})}_{\gamma p}$, and $T^{(\frac{1}{2})}_{\gamma n}$, where the production amplitudes $T^{(I)}_{\gamma N}$ are related to the $T^{(0,\pm)}_{\gamma N}$ via

$$\begin{aligned} T^{(\frac{3}{2})}_{\gamma N} &= T^{(\frac{3}{2})}_{\gamma p} = T^{(\frac{3}{2})}_{\gamma n} = T^{(+)}_{\gamma N} - T^{(-)}_{\gamma N},\\ T^{(\frac{1}{2})}_{\gamma p} &= T^{(0)}_{\gamma N} + \frac{1}{3}T^{(+)}_{\gamma N} + \frac{2}{3}T^{(-)}_{\gamma N},\\ T^{(\frac{1}{2})}_{\gamma n} &= T^{(0)}_{\gamma N} - \frac{1}{3}T^{(+)}_{\gamma N} - \frac{2}{3}T^{(-)}_{\gamma N}. \end{aligned} \tag{10}$$

The isospin parametrization is a natural choice when working in the isospin symmetric case of χPT; thus we perform the fits in this work using this basis. For comparison with experimental results, decomposition (9) in terms of the physical reaction channels is required.

The pion photoproduction amplitude $\mathcal{M} = \epsilon^\mu \mathcal{M}_\mu$, where ϵ^μ is the polarization vector of the photon, can be parametrized in terms of the so-called Ball amplitudes [71][1]

$$\mathcal{M}^\mu = \sum_{i=1}^{8} \bar{u}(p') B_i V_i^\mu u(p). \tag{11}$$

Here the coefficients B_i are scalar functions of the Mandelstam variables, and the basis structures V_i^μ comprise all independent matrices that can be formed using γ matrices and the polarization vector; they read

$$\begin{aligned} V_1^\mu &= \gamma^\mu\gamma_5, & V_2^\mu &= \gamma_5 P^\mu, & V_3^\mu &= \gamma_5 q^\mu, & V_4^\mu &= \gamma_5 k^\mu,\\ V_5^\mu &= \gamma^\mu \not{k}\gamma_5, & V_6^\mu &= \not{k}\gamma_5 P^\mu, & V_7^\mu &= \not{k}\gamma_5 q^\mu, & V_8^\mu &= \not{k}\gamma_5 k^\mu, \end{aligned} \tag{12}$$

where $P = 1/2\,(p + p')$. Note that the set of amplitudes (11) and (12) is not minimal. Imposing transversality $k_\mu \mathcal{M}^\mu = 0$ leads to the following conditions:

$$\begin{aligned} B_1 + B_6\, k\cdot P + B_7\, k\cdot q + B_8\, k^2 &= 0,\\ B_2\, k\cdot P + B_3\, k\cdot q + B_4\, k^2 + B_5\, k^2 &= 0. \end{aligned} \tag{13}$$

Thus, current conservation reduces the number of basis structures to six. Only four structures remain for real pion photoproduction due to the additional constraints $\epsilon\cdot k = 0$ and $k^2 = 0$, which can be chosen in the form of Chew-Goldberger-Low-Nambu (CGLN) amplitudes [72]:

$$\begin{aligned} \mathcal{M}^\mu &= \sum_{i=1}^{4} \bar{u}(p') A_i M_i^\mu u(p),\\ M_1^\mu &= -\frac{\mathrm{i}}{2}\gamma_5(\gamma^\mu \not{k} - \not{k}\gamma^\mu),\\ M_2^\mu &= 2\mathrm{i}\gamma_5\left(P^\mu k\cdot\left(q - \frac{1}{2}k\right) - \left(q^\mu - \frac{1}{2}k^\mu\right)k\cdot P\right),\\ M_3^\mu &= -\mathrm{i}\gamma_5(\gamma^\mu k\cdot q - \not{k} q^\mu),\\ M_4^\mu &= -2\mathrm{i}\gamma_5(\gamma^\mu k\cdot P - \not{k} P^\mu) - 2m_N M_1^\mu. \end{aligned} \tag{14}$$

In the c.m. frame, one can conveniently introduce another set of amplitudes in the gauge $\epsilon^0 = 0$ [72]:

$$\epsilon_\mu \bar{u}(p')\left(\sum_{i=1}^{4} A_i M_i^\mu\right) u(p) = \frac{4\pi\sqrt{s}}{m_N}\chi_f^\dagger\, \mathcal{F}\, \chi_i, \tag{15}$$

with

$$\begin{aligned} \mathcal{F} = {}& \mathrm{i}\,\boldsymbol{\sigma}\cdot\boldsymbol{\epsilon}\,\mathcal{F}_1 + \frac{\boldsymbol{\sigma}\cdot\boldsymbol{q}\,\boldsymbol{\sigma}\cdot(\boldsymbol{k}\times\boldsymbol{\epsilon})}{|\boldsymbol{q}|\,|\boldsymbol{k}|}\mathcal{F}_2\\ &+ \mathrm{i}\frac{\boldsymbol{\sigma}\cdot\boldsymbol{k}\,\boldsymbol{q}\cdot\boldsymbol{\epsilon}}{|\boldsymbol{q}|\,|\boldsymbol{k}|}\mathcal{F}_3 + \mathrm{i}\frac{\boldsymbol{\sigma}\cdot\boldsymbol{q}\,\boldsymbol{q}\cdot\boldsymbol{\epsilon}}{|\boldsymbol{q}|^2}\mathcal{F}_4, \end{aligned} \tag{16}$$

where $\boldsymbol{\sigma}$ are the Pauli matrices in spin space and χ_i ($\chi_f^\dagger$) is the Pauli spinor of the initial (final) nucleon.

The $\mathcal{F}_i$'s can be expanded in a multipole series [71,72]:

$$\begin{aligned} \mathcal{F}_1 &= \sum_{l=0}^{\infty}\{[l\,M_{l+} + E_{l+}]P'_{l+1}(x)\\ &\quad + [(l+1)M_{l-} + E_{l-}]P'_{l-1}(x)\},\\ \mathcal{F}_2 &= \sum_{l=1}^{\infty}[(l+1)M_{l+} + lM_{l-}]P'_l(x),\\ \mathcal{F}_3 &= \sum_{l=1}^{\infty}\{[E_{l+} - M_{l+}]P''_{l+1}(x) + [E_{l-} + M_{l-}]P''_{l-1}(x)\},\\ \mathcal{F}_4 &= \sum_{l=2}^{\infty}[M_{l+} - E_{l+} - M_{l-} - E_{l-}]P''_l(x), \end{aligned} \tag{17}$$

where $x = \cos(\theta)$, $P_l(x)$ is a Legendre polynomial of degree l, $P'_l(x) = \frac{\mathrm{d}P_l}{\mathrm{d}x}(x)$ is its first derivative, $P''_l(x)$ is the second derivative with respect to x, and l is the orbital angular momentum of the outgoing pion-nucleon system. The subscript $\pm$ denotes the total angular momentum $j = l \pm 1/2$.

[1]We work with Hilt's convention, given in Ref. [54], which is slightly different from Ball's original one.

Equation (17) can be inverted:

$$
\begin{aligned}
E_{l+} &= \int_{-1}^{1} \frac{\mathrm{d}x}{2(l+1)} \Big[P_l \mathcal{F}_1 - P_{l+1} \mathcal{F}_2 + \frac{l}{2l+1} \\
&\quad \times (P_{l-1} - P_{l+1}) \mathcal{F}_3 + \frac{l+1}{2l+3} (P_l - P_{l+2}) \mathcal{F}_4 \Big], \\
E_{l-} &= \int_{-1}^{1} \frac{\mathrm{d}x}{2l} \Big[P_l \mathcal{F}_1 - P_{l-1} \mathcal{F}_2 - \frac{l+1}{2l+1} \\
&\quad \times (P_{l-1} - P_{l+1}) \mathcal{F}_3 + \frac{l}{2l-1} (P_l - P_{l-2}) \mathcal{F}_4 \Big], \\
M_{l+} &= \int_{-1}^{1} \frac{\mathrm{d}x}{2(l+1)} \Big[P_l \mathcal{F}_1 - P_{l+1} \mathcal{F}_2 \\
&\quad - \frac{1}{2l+1} (P_{l-1} - P_{l+1}) \mathcal{F}_3 \Big], \\
M_{l-} &= \int_{-1}^{1} \frac{\mathrm{d}x}{2l} \Big[-P_l \mathcal{F}_1 + P_{l-1} \mathcal{F}_2 + \frac{1}{2l+1} (P_{l-1} - P_{l+1}) \mathcal{F}_3 \Big].
\end{aligned} \tag{18}
$$

Here, we suppress the x dependence of the Legendre polynomials P_l for the sake of brevity.

To calculate multipole amplitudes, we proceed as follows: First, we express the pion photoproduction amplitude in terms of the Ball amplitudes [Eq. (11)]. Then, we rewrite the B_i's in terms of A_i's to obtain the representation of the amplitude in the minimal basis [Eq. (14)]. Finally, we use the coefficients A_i to calculate $\mathcal{F}_1 - \mathcal{F}_4$. The relations between these representations are given in Appendix A.

Next, we provide the expressions for the unpolarized differential cross section and linear polarization asymmetry. The differential cross section for pion photoproduction is given by

$$
\frac{\mathrm{d}\sigma}{\mathrm{d}\Omega} = \frac{1}{64\pi^2 s} \frac{|\boldsymbol{q}|}{|\boldsymbol{k}|} |\overline{\mathcal{M}}|^2, \tag{19}
$$

with the unpolarized squared matrix element $|\overline{\mathcal{M}}|^2$,

$$
|\overline{\mathcal{M}}|^2 = \frac{1}{4} \sum_{\lambda=-1}^{1} \sum_{s,s'=-1}^{1} |\epsilon_\mu(k,\lambda) \mathcal{M}^\mu(k,p,s,p',s',q)|^2, \tag{20}
$$

where again λ is the helicity of the photon, s (s') is the spin of the incoming (outgoing) nucleon, and the factor of $1/4$ arises from averaging over helicity and spin of the incoming particles. The linearly polarized photon asymmetry Σ is given by

$$
\Sigma = \frac{\mathrm{d}\sigma_\perp - \mathrm{d}\sigma_\parallel}{\mathrm{d}\sigma_\perp + \mathrm{d}\sigma_\parallel}, \tag{21}
$$

where $\mathrm{d}\sigma_\perp$ and $\mathrm{d}\sigma_\parallel$ refer to the differential cross section for photon polarizations perpendicular and parallel to the reaction plane, respectively.

III. EFFECTIVE LAGRANGIAN AND POWER COUNTING

The calculation of observables in chiral perturbation theory is based on Feynman rules derived from the effective Lagrangian. In general, it contains an infinite number of terms with a rising number of derivatives and/or pion masses. At the maximal order we are working with, the terms of the effective Lagrangian relevant for the calculation of pion photoproduction read

$$
\begin{aligned}
\mathcal{L}_{\text{eff}} &= \mathcal{L}^{(2)}_{\pi\pi} + \mathcal{L}^{(4)}_{\pi\pi} + \mathcal{L}^{(1)}_{\pi N} + \mathcal{L}^{(2)}_{\pi N} + \mathcal{L}^{(3)}_{\pi N} + \mathcal{L}^{(1)}_{\pi N\Delta} \\
&\quad + \mathcal{L}^{(2)}_{\pi N\Delta} + \mathcal{L}^{(3)}_{\pi N\Delta} + \mathcal{L}^{(1)}_{\pi\Delta} + \mathcal{L}^{(2)}_{\pi\Delta},
\end{aligned} \tag{22}
$$

where we do not distinguish between HB and covariant notation at this point.

In the mesonic sector, the building blocks are the pion field $U = u^2$ with

$$
\begin{aligned}
U(x) &= 1 + \mathrm{i} \frac{\boldsymbol{\tau} \cdot \boldsymbol{\pi}}{F} - \frac{\pi^2}{2F^2} - \mathrm{i}\alpha \frac{\pi^2 \, \boldsymbol{\tau} \cdot \boldsymbol{\pi}}{F^3} \\
&\quad + \left(\alpha - \frac{1}{8} \right) \frac{\pi^4}{F^4} + \mathcal{O}(\pi^5),
\end{aligned} \tag{23}
$$

where F is the pion decay constant in the chiral limit and α is an arbitrary unphysical parameter from the parametrization of the pion field. The covariant derivative acting on the pion field ∇_μ is defined as

$$
\begin{aligned}
\nabla_\mu U &= \partial_\mu U - \mathrm{i} r_\mu U + \mathrm{i} U l_\mu, \\
l_\mu &= v_\mu - a_\mu, \quad r_\mu = v_\mu + a_\mu,
\end{aligned} \tag{24}
$$

where $v_\mu = -e Q_N A_\mu = -e \frac{\mathbb{1} + \tau_3}{2} A_\mu$ is the vector source with the electric charge $e \approx 0.303$ and the electromagnetic field A_μ, and a_μ is the axial source. Furthermore, we introduce $\chi = \mathrm{diag}(M^2, M^2)$ and M is the pion mass to leading order in quark masses. We also introduce the field combinations

$$
\begin{aligned}
\chi_\pm &= u^\dagger \chi u^\dagger \pm u \chi^\dagger u, \quad F_L^{\mu\nu} = \partial^\mu l^\nu - \partial^\nu l^\mu - \mathrm{i}[l^\mu, l^\nu], \\
F_R^{\mu\nu} &= \partial^\mu r^\nu - \partial^\nu r^\mu - \mathrm{i}[r^\mu, r^\nu].
\end{aligned} \tag{25}
$$

The relevant parts of the leading and next-to-leading pionic Lagrangian read [73]

$$
\begin{aligned}
\mathcal{L}^{(2)}_{\pi\pi} &= \frac{F^2}{4} \mathrm{tr}(\nabla_\mu U \nabla^\mu U^\dagger) + \frac{F^2}{4} \mathrm{tr}(\chi_+), \\
\mathcal{L}^{(4)}_{\pi\pi} &= \frac{l_3}{16} \mathrm{tr}(\chi_+)^2 + \frac{l_4}{16} (2\mathrm{tr}(\nabla_\mu U (\nabla^\mu U)^\dagger) \mathrm{tr}(\chi_+) \\
&\quad + \mathrm{tr}(2((\chi U^\dagger)^2 + (U \chi^\dagger)^2) - 4\chi^\dagger \chi - \chi_-^2)) \\
&\quad + \mathrm{i} \frac{l_6}{2} \mathrm{tr}(F_{R,\mu\nu} \nabla^\mu U (\nabla^\nu U)^\dagger + F_{L,\mu\nu} (\nabla^\mu U)^\dagger \nabla^\nu U).
\end{aligned} \tag{26}
$$

Introducing nucleons, we give the definitions of

$$
\begin{aligned}
&D_\mu = \partial_\mu - \Gamma_\mu, \quad \Gamma_\mu = \frac{1}{2} \{ u^\dagger (\partial_\mu - \mathrm{i} r_\mu) u + u (\partial_\mu - \mathrm{i} l_\mu) u^\dagger \}, \\
&u_\mu = \mathrm{i} (u^\dagger (\partial_\mu - \mathrm{i} r_\mu) u - u (\partial_\mu - \mathrm{i} l_\mu) u^\dagger), \\
&F^\pm_{\mu\nu} = u^\dagger F^R_{\mu\nu} u \pm u F^L_{\mu\nu} u^\dagger, \quad \tilde{F}^\pm_{\mu\nu} = F^\pm_{\mu\nu} - \frac{1}{2} \mathrm{Tr}(F^\pm_{\mu\nu}).
\end{aligned} \tag{27}
$$

The leading-order pion-nucleon Lagrangian in the covariant approach is given by

$$\mathcal{L}_{\pi N}^{(1)} = \bar{\Psi}_N \Big(\mathrm{i} \not{D} - m + \frac{g}{2} \not{u} \gamma_5 \Big) \Psi_N, \tag{28}$$

where m and g are the bare nucleon mass and axial coupling constant. Other relevant parts of the covariant πN Lagrangian read (see, e.g., Ref. [74])

$$\begin{aligned}
\mathcal{L}_{\pi N}^{(2)} &= \bar{\Psi}_N \left\{ c_1 \mathrm{tr}(\chi_+) + \frac{c_6}{8m_N} F^+_{\mu\nu} \sigma^{\mu\nu} + \frac{c_7}{8m_N} \mathrm{tr}(F^+_{\mu\nu}) \sigma^{\mu\nu} \right\} \Psi_N, \\
\mathcal{L}_{\pi N}^{(3)} &= \bar{\Psi}_N \left\{ \frac{d_6}{2m_N} (\mathrm{i}[D^\mu, \tilde{F}^+_{\mu\nu}] D^\nu + \mathrm{H.c.}) + \frac{d_7}{2m_N} (\mathrm{i}[D^\mu, \mathrm{tr}(F^+_{\mu\nu})] D^\nu + \mathrm{H.c.}) + \frac{d_8}{2m_N} (\mathrm{i} \boldsymbol{\varepsilon}^{\mu\nu\alpha\beta} \mathrm{tr}(\tilde{F}^+_{\mu\nu} u_\alpha) D_\beta + \mathrm{H.c.}) \right. \\
&\quad + \frac{d_9}{2m_N} (\mathrm{i} \boldsymbol{\varepsilon}^{\mu\nu\alpha\beta} \mathrm{tr}(F^+_{\mu\nu}) u_\alpha D_\beta + \mathrm{H.c.}) + \frac{d_{16}}{2} \gamma^\mu \gamma_5 \mathrm{tr}(\chi_+) u_\mu + \mathrm{i} \frac{d_{18}}{2} \gamma^\mu \gamma_5 [D_\mu, \chi_-] \\
&\quad \left. - \frac{d_{20}}{8m_N^2} (\mathrm{i} \gamma^\mu \gamma_5 [\tilde{F}^+_{\mu\nu}, u_\alpha] D^{\alpha\nu} + \mathrm{H.c.}) + \mathrm{i} \frac{d_{21}}{2} \gamma^\mu \gamma_5 [\tilde{F}^+_{\mu\nu}, u^\nu] + \frac{d_{22}}{2} \gamma^\mu \gamma_5 [D^\nu, F^-_{\mu\nu}] \right\} \Psi_N,
\end{aligned}$$

with $\sigma^{\mu\nu} = \frac{\mathrm{i}}{2}[\gamma^\mu, \gamma^\nu]$. We use the convention $\boldsymbol{\varepsilon}^{0123} = -1$.

In the heavy-baryon formalism, the nucleon momentum is split according to

$$p_\mu = m_N v_\mu + P_\mu, \tag{29}$$

where the first part is a large piece close to the on-shell kinematics and the second part P_μ is a soft residual contribution $v \cdot P \ll m_N$. The vector v_μ is the four-velocity of the nucleon with the properties $v^2 = 1$, $v^0 \geqslant 1$ and can be conveniently chosen as $v = (1, 0, 0, 0)$. The nucleon field Ψ_N is split into the so-called light and heavy fields,

$$N_v(x) = \mathrm{e}^{\mathrm{i} m_N v \cdot x} P_v^+ \Psi_N(x) \text{ and } h_v(x) = \mathrm{e}^{\mathrm{i} m_N v \cdot x} P_v^- \Psi_N(x), \tag{30}$$

which are eigenstates of $\not{v}$, with the projectors

$$P_v^\pm = \tfrac{1}{2}(1 \pm \not{v}). \tag{31}$$

In the heavy-baryon formalism, any bilinear $\bar{\Psi} \Gamma \Psi$ with $\Gamma \in \{1, \gamma_5, \gamma_\mu, \gamma_5 \gamma_\mu, \sigma_{\mu\nu}\}$ can be expressed in terms of the velocity v^μ and the Pauli-Lubanski spin vector:

$$S_\mu = \frac{\mathrm{i}}{2} \gamma_5 \sigma_{\mu\nu} v^\nu. \tag{32}$$

The relevant terms of the Lagrangians up to third order read [74]

$$\begin{aligned}
\hat{\mathcal{L}}_{\pi N}^{(1)} &= \bar{N} (\mathrm{i} v \cdot D + g S \cdot u) N, \\
\hat{\mathcal{L}}_{\pi N}^{(2)} &= \bar{N} \left(c_1 \mathrm{tr}(\chi_+) - \frac{\mathrm{i}}{4m_N} [\hat{c}_6 [S^\mu, S^\nu] F^+_{\mu\nu} + \hat{c}_7 [S^\mu, S^\nu] \mathrm{tr}(F^+_{\mu\nu})] \right) N, \\
\hat{\mathcal{L}}_{\pi N}^{(3)} &= \bar{N} \big(\hat{d}_6 [D^\mu, \tilde{F}^+_{\mu\nu}] v^\nu + \hat{d}_7 [D^\mu, \mathrm{tr}(F^+_{\mu\nu})] v^\nu + \hat{d}_8 \mathrm{tr}(\tilde{F}^+_{\mu\nu} u_\alpha) \boldsymbol{\varepsilon}^{\mu\nu\alpha\beta} v_\beta + \hat{d}_9 \mathrm{tr}(F^+_{\mu\nu}) u_\alpha \boldsymbol{\varepsilon}^{\mu\nu\alpha\beta} v_\beta \\
&\quad + \hat{d}_{16} S \cdot u \mathrm{tr}(\chi_+) + \mathrm{i} \hat{d}_{18} [S \cdot D, \chi_-] + \mathrm{i} \hat{d}_{20} S^\mu v^\nu [\tilde{F}^+_{\mu\nu}, v \cdot u] + \mathrm{i} \hat{d}_{21} S^\mu [\tilde{F}^+_{\mu\nu}, u^\nu] + \hat{d}_{22} S^\mu [D^\nu, F^-_{\mu\nu}] \big) N \\
&\quad + \frac{1}{2m_N} \bar{N} ((v \cdot D)^2 - D^2 - \mathrm{i} g \{S \cdot D, v \cdot u\}) N.
\end{aligned} \tag{33}$$

The prefactor of $1/m_N$ in the c_i parts in $\hat{\mathcal{L}}_{\pi N}^{(2)}$ should not be interpreted as a $1/m_N$ correction; it originates from the definition of the constants $\hat{c}_6$ and $\hat{c}_7$, which are dimensionless when defined this way. Unlike the usual treatment of the single nucleon sector in the literature, we from now on consider the $1/m_N$ corrections as $1/m_N \sim 1/\Lambda^2$, where Λ is the hard scale (see below), so that they start to appear at the third instead of the second order. The $1/m_N^2$ are, therefore, shifted beyond the order with which we are working. This is a common practice in studies of the nuclear forces [75] and is referred to as NN counting in this work. Also, note that the heavy-baryon LECs $\hat{c}_6$ and $\hat{c}_7$ are not the same as the covariant constants, but they absorb $1/m_N$ shifts from the leading-order Lagrangian via $\hat{c}_6 = c_6 + 1$, $\hat{c}_7 = c_7$.

The Δ resonance is introduced as an explicit degree of freedom by an isospin-3/2 Rarita-Schwinger spinor $\bar{\Psi}^\mu_{\Delta,i}$, which satisfies $\tau_i \Psi^i_{\Delta,\mu} = 0$ [57]. Given the definitions

$$D^{ij}_\mu = \partial_\mu \delta^{ij} + \Gamma^{ij}_\mu, \quad \Gamma^{ij}_\mu = \delta^{ij} \Gamma_\mu - \mathrm{i} \boldsymbol{\varepsilon}^{ijk} \mathrm{tr}(\tau_k \Gamma^\mu), \quad u^{ij}_\mu = \xi^{ik}_{3/2} u_\mu \xi^{kj}_{3/2}, \tag{34}$$

with the isospin projectors

$$\xi_{ij}^{3/2} = \frac{2}{3}\delta_{ij} - \frac{\mathrm{i}}{3}\boldsymbol{\epsilon}_{ijk}\tau_k, \quad \xi_{ij}^{1/2} = \frac{1}{3}\delta_{ij} + \frac{\mathrm{i}}{3}\boldsymbol{\epsilon}_{ijk}\tau_k, \tag{35}$$

the leading covariant $\pi\Delta$ Lagrangian reads [57,76]

$$\begin{aligned}\mathcal{L}_{\pi\Delta}^{(1)} = &-\bar{\Psi}_{\Delta,i}^{\mu}\Big\{(\mathrm{i}\not{D}^{ij} - \mathring{m}_\Delta\delta^{ij})g_{\mu\nu} - \mathrm{i}\big(\gamma_\mu D_\nu^{ij} + \gamma_\nu D_\mu^{ij}\big) + \mathrm{i}\gamma_\mu\not{D}^{ij}\gamma_\nu + \mathring{m}_\Delta\gamma_\mu\gamma_\nu\delta^{ij} \\ &+ \frac{\mathring{g}_1}{2}g_{\mu\nu}\not{u}^{ij}\gamma_5 + \frac{\mathring{g}_2}{2}\big(\gamma_\mu u_\nu^{ij} + u_\mu^{ij}\gamma_\nu\big)\gamma_5 + \frac{\mathring{g}_3}{2}\gamma_\mu\not{u}^{ij}\gamma_5\gamma_\nu\Big\}\Psi_{\Delta,j}^{\nu},\end{aligned} \tag{36}$$

where $\mathring{m}_\Delta$ is the bare Δ mass and $\mathring{g}_1$, $\mathring{g}_2$, $\mathring{g}_3$ are the bare leading-order coupling constants. For pion photoproduction, only $\mathring{g}_1$ is relevant, whereas the constants $\mathring{g}_2$ and $\mathring{g}_3$ are off-shell parameters, which do not contribute if the Δ particle is on shell and result only in shifts of LECs.

The only term from the second-order $\pi\Delta$ Lagrangian relevant for our calculation is

$$\mathcal{L}_{\pi\Delta}^{(2)} = -\mathrm{i}c_1^{\Delta}\bar{\Psi}_{\Delta,\mu}^{i}\,\mathrm{Tr}\,(\chi_+)\sigma^{\mu\nu}\Psi_{\Delta,\nu}^{i}, \tag{37}$$

which enters barely the renormalization of the Δ mass.

We also need to take into account the nucleon-to-Δ transition Lagrangian $\mathcal{L}_{\pi N\Delta}$ up to third order. Again, we only give the relevant terms for pion photoproduction up to our working order [57,77]:

$$\begin{aligned}\mathcal{L}_{\pi N\Delta}^{(1)} =& h\big(\bar{\Psi}_{\Delta,i}^{\mu}\Theta_{\mu\nu}(z_0)w_i^{\nu}\Psi_N + \bar{\Psi}_N w_i^{\nu\dagger}\Theta_{\nu\mu}(z_0)\Psi_{\Delta,i}^{\mu}\big), \\ \mathcal{L}_{\pi N\Delta}^{(2)} =& \mathrm{i}\frac{b_1}{2}\bar{\Psi}_{\Delta,i}^{\mu}\Theta_{\mu\nu}(z_1)F_i^{+,\nu\alpha}\gamma_\alpha\gamma_5\Psi_N + \mathrm{i}b_3\bar{\Psi}_{\Delta,i}^{\mu}\Theta_{\mu\nu}(z_3)w_i^{\nu\alpha}\gamma_\alpha\Psi_N - \frac{b_6}{m}\bar{\Psi}_{\Delta,i}^{\mu}\Theta_{\mu\nu}(z_6)w_i^{\nu\alpha}D_\alpha\Psi_N + \cdots + \mathrm{H.c.}, \\ \mathcal{L}_{\pi N\Delta}^{(3)} =& \frac{h_1}{m}\bar{\Psi}_{\Delta,i}^{\mu}\Theta_{\mu\nu}(y_1)F_i^{+,\nu\alpha}\gamma_5 D_\alpha\Psi_N - \mathrm{i}\frac{h_{15}}{2}\bar{\Psi}_{\Delta,i}^{\mu}\Theta_{\mu\nu}(y_{15})\,\mathrm{Tr}([D^\alpha, F^{+,\nu\beta}]\tau^i)\sigma_{\alpha\beta}\gamma_5\Psi_N \\ &+ \mathrm{i}\frac{h_{16}}{2m}\bar{\Psi}_{\Delta,i}^{\mu}\Theta_{\mu\nu}(y_{16})\,\mathrm{Tr}([D^\alpha, F^{+,\nu\beta}]\tau^i)\gamma_\beta\gamma_5 D_\alpha\Psi_N + \cdots + \mathrm{H.c.},\end{aligned} \tag{38}$$

where h, b_i, and h_i are LECs and

$$w_i^{\mu} = \frac{1}{2}\,\mathrm{Tr}(\tau_i u^\mu), \quad w_i^{\mu\nu} = \frac{1}{2}\,\mathrm{Tr}(\tau_i[D^\mu, u^\nu]), \quad F_{i,\mu\nu}^{\pm} = \frac{1}{2}\,\mathrm{Tr}(\tau_i F_{\mu\nu}^{\pm}), \quad \Theta_{\mu\nu}(z) = g_{\mu\nu} + z\gamma_\mu\gamma_\nu. \tag{39}$$

$\Theta_{\mu\nu}(z)$ is an off-shell function with the off-shell parameter z. It was shown in Ref. [78] that the dependence on the off-shell parameters can be eliminated by a redefinition of the LECs up to higher-order corrections. Thus, we set them to zero in our calculations. The Δ propagator [79] derived from the Lagrangian (36) reads

$$\mathcal{G}_{\Delta,ij}^{\mu\nu}(p) = -\frac{\mathrm{i}(\not{p} + \mathring{m}_\Delta)}{p^2 - \mathring{m}_\Delta^2}\left(g^{\mu\nu} - \frac{1}{d-1}\gamma^\mu\gamma^\nu + \frac{1}{d-1}\frac{p^\mu\gamma^\nu - p^\nu\gamma^\mu}{\mathring{m}_\Delta} + \frac{d-2}{d-1}\frac{p^\mu p^\nu}{\mathring{m}_\Delta^2}\right)\xi_{ij}^{3/2} \tag{40}$$

with the isospin projector

$$\xi_{ij}^{3/2} = \frac{2}{3}\delta_{ij} - \frac{\mathrm{i}}{3}\boldsymbol{\epsilon}_{ijk}\tau_k. \tag{41}$$

We also give our power-counting scheme. In the Δ-less case, we employ

$$Q = \frac{q}{\Lambda} \in \left\{\frac{M_\pi}{\Lambda}, \frac{k}{\Lambda}\right\} \text{ with } \Lambda \in \{\Lambda_b, 4\pi F_\pi\}, \tag{42}$$

where k is an arbitrary three-momentum (of a meson or a baryon), F_π is the pion decay constant, and Λ_b is the breakdown scale of the chiral expansion. In the Δ-full theory, we introduce the Δ-nucleon-mass splitting $\Delta = m_\Delta - m_N$, which we count as an additional small parameter of order $\mathcal{O}(M_\pi)$, but which does not vanish in the chiral limit. In the Δ-full case, we use the SSE counting scheme [57]

$$\epsilon \in \left\{\frac{M_\pi}{\Lambda}, \frac{k}{\Lambda}, \frac{\Delta}{\Lambda}\right\} \text{ with } \Lambda \in \{\Lambda_b, 4\pi F_\pi\}, \tag{43}$$

with ϵ as the new expansion parameter in the Δ-full case in contrast to Q in the Δ-less theory.

The order D of any Feynman diagram can be computed according to the formula [80]

$$D = 1 + 2L + \sum_n (2n-2)V_{2n}^M + \sum_d (d-1)V_d^B, \tag{44}$$

where L is the number of loops, V_{2n}^M is the number of purely mesonic vertices of order $2n$, and V_d^B is the number of vertices involving baryons of order d.

According to Eq. (44), up to order $\mathcal{O}(Q^3)$ in the Δ-less scheme, a number of tree-level and loop contributions have to be taken into account. At order $\mathcal{O}(\epsilon^2)$ [$\mathcal{O}(\epsilon^3)$], the leading (subleading) tree-level diagrams with Δ are included. The corresponding sets of diagrams can be found in Appendix B of Ref. [1].

The one-loop diagrams with Δ that appear at order $\mathcal{O}(\epsilon^3)$ are given in Appendix B of the present paper.

At this point, it is instructive to compare the SSE scheme with the δ counting. In the δ-counting scheme, the leading tree-level diagrams with Δ are of order $\mathcal{O}(\delta^5) \equiv \mathcal{O}(p^{5/2})$. Therefore, calculations at order $\mathcal{O}(\delta^6) \equiv \mathcal{O}(p^3)$ (see, e.g., Refs. [60–62]) correspond to order $\mathcal{O}(Q^3 + \epsilon^2)$ in the SSE.

Next, one-loop diagrams with a single Δ line are counted as $\mathcal{O}(\delta^7) \equiv \mathcal{O}(p^{7/2})$ (see, e.g., Ref. [59]), whereas in the SSE they appear at order $\mathcal{O}(\epsilon^3)$ together with the loop graphs involving two and three Δ lines. Note that the diagrams with a single Δ line do not form a gauge-invariant set so that the result depends on a prescription one follows to restore gauge invariance. However, even if we consider the gauge-invariant set of diagrams containing all one-loop graphs with one Δ line as a subset (diagrams in Figs. 9, 10, and 12), i.e., the contribution proportional to $h_A^2 g_A$, there will remain diagrams proportional to $h_A^2 g_1$ (diagrams in Figs. 11 and 13) that are of order $\mathcal{O}(\epsilon^3)$ according to the SSE.

In the Δ region, power counting has to be modified as compared to the threshold region as was first shown in Ref. [63], where the δ counting for nucleon Compton scattering was considered. For pion photoproduction, such a modification was discussed in Ref. [81] for the case of the δ counting and in Ref. [1] for the case of the SSE. The modification is caused by the enhancement of the Δ pole diagrams near the pole by a factor

$$\gamma = \frac{\Delta}{|\mathrm{Im}(m_\Delta)|}. \tag{45}$$

In the present work, we do not apply this modification and follow the power counting given by Eq. (44) because in our case, the Δ region constitutes only a small part of the whole analyzed energy domain. Since the Δ pole contributions are taken into account anyway, the effect of not promoting them to lower orders may only result in a slight increase of the theoretical errors.

As mentioned above, the $1/m_N$ corrections in the heavy-baryon scheme are treated following the NN counting, so that $\frac{q}{m_N} \sim \mathcal{O}(Q^2)$.

IV. RENORMALIZATION

In this section, we discuss the subtleties of renormalization, i.e., all steps necessary to remove unphysical infinities and possible power-counting breaking terms from the theory.

A. Renormalization of subprocesses

To relate the bare constants of the effective Lagrangian to their physical counterparts, we must consider various subprocesses of pion photoproduction. We take care of the appearing integrals and their ultraviolet (UV) divergences by dimensional regularization. Also, we choose to renormalize the masses, wave functions, and coupling constants using the on-shell renormalization. Our renormalization scheme and the renormalization conditions for the pion, nucleon, and Δ self-energies, pion decay constant, πNN, $\pi N\Delta$, and $\pi\Delta\Delta$ coupling constants, the nucleon magnetic moments, and the electromagnetic $N\Delta$ transition form factor were described in detail in Ref. [1]. For completeness, we provide the expressions for all counterterms needed in our calculation in Appendix C. Note that loops with internal Δ lines appearing at order ϵ^3 were not included in Ref. [1]. The corresponding additional contribution to the counterterms are indicated by the superscript Δ, e.g., $\delta m_N^{(3,\Delta)}$.

Since a part of the Δ region is included in our analysis, the Δ width has to be taken into account. Note that in contrast to the energy-dependent Δ width obtained by a resummation of the Δ self-energy graphs typically used in the δ-counting scheme, we introduce the energy-independent Δ width on the level of the effective Lagrangian using the so-called complex mass scheme [82–85]. This allows us to stay within the perturbation theory framework. The Δ-mass renormalization within the complex mass scheme is performed in exactly the same manner as in Ref. [1].

B. Renormalization of the photoproduction LECs

Additionally to the UV divergences removed by on-shell renormalization of the subprocesses, it is necessary to perform a renormalization of the photoproduction LECs to absorb the remaining divergences and (possibly) power-counting breaking terms. In the covariant approach, we employ the EOMS renormalization scheme [52]. The LEC shifts are defined as

$$d_i = \bar{d}_i + \beta_{d_i} \frac{\bar{\lambda}}{F_\pi^2} \tag{46}$$

in the covariant approach and as

$$\hat{d}_i = \hat{d}_i^r + \beta_{\hat{d}_i} \frac{\bar{\lambda}}{F_\pi^2} \tag{47}$$

in the HB approach, where

$$\bar{\lambda} = \frac{1}{16\pi^2}\left[\frac{1}{d-4} + \frac{1}{2}(-1 + \gamma_E - \ln 4\pi)\right], \tag{48}$$

and d is the space-time dimension. The renormalized LECs are denoted by the superscript "r" in the HB approach and by the bar in the covariant case. Note that, in this work, we use a more standard definition of $\bar{d}_i$ as compared to Ref. [1].

The renormalization scale μ in all integrals (see Appendix C 1) is set to $\mu = m_N$ ($\mu = M_\pi$) for the covariant (heavy-baryon) scheme to be consistent with traditional choices in the literature.

In the Δ-less HB sector, the β functions were given in Ref. [86]:

$$\begin{aligned} &\beta_{\hat{d}_8} = 0, \quad \beta_{\hat{d}_9} = 0, \quad \beta_{\hat{d}_{20}} = g_A + g_A^3, \\ &\beta_{\hat{d}_{21}} = -g_A^3, \quad \beta_{\hat{d}_{22}} = 0. \end{aligned} \tag{49}$$

In the covariant approach, they can easily be derived by expanding the UV divergent piece of the whole scattering amplitude in the small scales up to the working order. In the Δ-less approach, they are found to vanish,

$$\beta_{d_8} = \beta_{d_9} = \beta_{d_{20}} = \beta_{d_{21}} = \beta_{d_{22}} = 0, \tag{50}$$

but for the full ϵ^3 amplitude, they read

$$\begin{aligned} &\beta_{d_8} = \tfrac{19}{54} g_A h_A^2 - \tfrac{55}{729} g_1 h_A^2, \quad \beta_{d_9} = -\tfrac{97}{324} g_A h_A^2 + \tfrac{55}{1458} g_1 h_A^2, \\ &\beta_{d_{20}} = \tfrac{47}{162} g_A h_A^2 - \tfrac{2555}{1458} g_1 h_A^2, \\ &\beta_{d_{21}} = -\tfrac{823}{162} g_A h_A^2 + \tfrac{10}{27} g_1 h_A^2, \quad \beta_{d_{22}} = \tfrac{40}{27} g_A h_A^2 - \tfrac{425}{243} g_1 h_A^2. \end{aligned} \tag{51}$$

TABLE I. Particle masses (in MeV) and leading-order coupling constants used in this work. Unless specified, the values are taken from the Particle Data Group (PDG) [91].

M_π	m_N	m_Δ (fit)	e	F_π (MeV)	g_A	h_A	g_1
138.03	938.27	1219.3 − 53.7 i	0.303	92.1	1.289 [92]	1.43 [85,93]	−1.21 [85]

Here and in what follows, g_A and h_A are the nucleon axial coupling and the $\pi N\Delta$ coupling constant, respectively. In the EOMS scheme, the power-counting violating terms must be subtracted by shifting the LECs. Up to the order with which we are working, it can easily be argued that power-counting violating terms cannot occur, since the symmetry constraints allow contact interactions in the photoproduction sector starting only from order Q^3. We explicitly checked the absence of power-counting violating terms by replacing all occurring integrals in the Q^3 amplitude by their infrared regular part and performing an explicit expansion in the small scales. We verified that all power-counting violating terms cancel out, which provides a valuable consistency check, because nontrivial cancellations are analytically fulfilled. In the Δ-full approach at order ϵ^3, we refrained from repeating this exercise, since the same argument as in the Δ-less case holds and performing the comparable test would require considerably more effort. We conclude that for our study, the EOMS scheme is effectively equivalent to the $\widetilde{MS}$ scheme [52,73].

As explained in Ref. [1], the constants b_3, b_6, h_{15}, and h_{16} are redundant at our working order. The shifts to absorb these LECs in the covariant order-ϵ^3 amplitude through a redefinition of h_A, b_1, and h_1 are given by $d_i \to d_i + \delta_{d_i}$ with

$$\delta_{d_8} = \delta_{d_{20}} = -\delta_{d_{21}} = \frac{-b_1(b_3+b_6)+2h_A(h_{15}+h_{16})}{9},$$
$$\delta_{d_9} = \delta_{d_{22}} = 0. \tag{52}$$

V. RESULTS AND DISCUSSION

In this section, we present the results of our calculation. We used our own code written in *Mathematica* [87], FORM [88], and FORTRAN and relied on LoopTools [89] and on the *X* package [90] for the numerical evaluation of loop integrals.

A. Low-energy constants

In the Δ-less theory, there are four independent parameters to be determined, which are d_8, d_9, d_{20}, and $d_{21;22} = d_{21} - d_{22}/2$. Note that while the numerical values of LECs are, in general, different in the HB and covariant approaches, the fitting procedure is similar. Thus, when we discuss points applicable to both formalisms in the Δ-less fits, we simply use d_i for referring to both renormalized parameters $\bar{d}_i$ and $\hat{d}_i^r$. Note that one cannot assess the constants d_{21} and d_{22} individually in real pion photoproduction; we can determine only the combination $d_{21;22}$. When including the leading-order Δ tree diagrams of order ϵ^2, the additional constant b_1 enters the amplitude. b_1 corresponds to the leading-order $\gamma N\Delta$ coupling constant. At order ϵ^3, the additional coupling h_1, the subleading $\gamma N\Delta$ coupling is introduced. The values of the constants taken from other sources are collected in Table I. The value of the Δ mass was determined from a fit to the order-ϵ^2 amplitude as described in Ref. [1].

The numerical values of LECs in the covariant and in the heavy-baryon approaches are, in general, not directly comparable. First, the values are related by $1/m_N$ corrections, which originate from the construction of the HB Lagrangian, where a strict expansion in terms of the inverse nucleon mass is done, such that the dependence on m_N is shifted to a series of additional contact interactions suppressed by powers in $1/m_N$. Note that the corrections are only relevant if the working order is beyond the order at which the LECs appear first. For example, the values of b_1 in both frameworks can be compared directly if only the leading Δ tree contributions (order ϵ^2) are included, because the difference starts to arise from $1/m_N$ corrections, which, however, are beyond the working order. For LECs appearing at the loop level, an extra shift generated by the infrared regular (IR) part of the loop integrals must be considered (the way of calculating the IR part of a loop integral is described in, e.g., Ref. [52]). In the covariant framework, the IR part gives rise to additional numerical contributions, which affect the fitted values of the LECs. Because these parts are absent in the HB approach, the covariant LECs cannot be compared with the HB values, even if inverse nucleon mass corrections are irrelevant. However, the contributions of the IR part to the covariant LECs can be calculated analytically and switched off in order to restore the same meaning of the LECs in the HB and covariant approaches. We determined these IR shifts by replacing the integrals of the covariant amplitude by their corresponding IR term and adjusting the constants in such a way that the obtained expression vanishes. The shifts we found for the relevant d_i's are given by

$$\Delta d_8^{\rm IR} = \bar{d}_8 - \hat{d}_8 = \frac{g_A}{128F_\pi^2\pi^2}\left(3+g_A^2\right),$$
$$\Delta d_9^{\rm IR} = \bar{d}_9 - \hat{d}_9 = \frac{g_A}{128F_\pi^2\pi^2}\left(-1+g_A^2\right),$$
$$\Delta d_{20}^{\rm IR} = \bar{d}_{20} - \hat{d}_{20} = \frac{g_A}{96F_\pi^2\pi^2}\left[6+11g_A^2+3\left(1+g_A^2\right)\left(1-\gamma_E+\ln(4\pi)+\ln\left(M_\pi^2/m_N^2\right)\right)\right],$$
$$\Delta d_{21;22}^{\rm IR} = \bar{d}_{21;22} - \hat{d}_{21;22} = -\frac{g_A}{96F_\pi^2\pi^2}\left[3+8g_A^2+3g_A^2\left(1-\gamma_E+\ln(4\pi)+\ln\left(M_\pi^2/m_N^2\right)\right)\right], \tag{53}$$

where we recall that the constants with the hat refer to HB parameters.

The numerical differences between LECs determined in a Δ-less and a Δ-full framework are expected to be qualitatively described in terms of resonance saturation by calculating the dominating leading-order contributions of the Δ to specific LECs, as stated in the decoupling theorem [94]. In our case, this is accomplished by expanding the order-ϵ^2 Δ-full tree diagrams in inverse powers of $\Delta \equiv m_\Delta - m_N$ and matching the obtained expressions with the contact term structures of the Δ-less theory. This procedure yields

$$\delta d_8(\Delta) = -\delta d_{21;22}(\Delta) = -\frac{h_A b_1}{9\Delta}, \quad \delta d_9(\Delta) = \delta d_{20}(\Delta) = 0, \tag{54}$$

with $\delta d_i(\Delta) = \bar{d}_i^{\not\Delta} - \bar{d}_i^{\Delta}$ denoting the difference between the constant $\bar{d}_i$ in the Δ-less (superscript $\not\Delta$) and Δ-full (superscript Δ) approaches.

B. Fitting procedure and Bayesian uncertainties

Ideally, one would fit the LECs to the whole set of available pion photoproduction data in the relevant energy range. However, analyzing all the data requires a lot of effort and is an art of its own, since there is a lot of data available on the photoproduction process. This is why we choose to fit to the multipoles of the partial-wave analysis (PWA) from Mainz, the MAID2007 model [95], which is a more pragmatic approach. Furthermore, we only fit to the real part of the multipoles, because the imaginary part follows from unitarity as stated by Watson's theorem [96] and does not provide new information. We fit to the multipoles in the isospin channels, which is a natural choice because isospin-breaking effects are not considered in this work. The four physical reaction channels are linear combinations of the isospin channels. In the following, we remark on several points relevant for the fits.

1. Uncertainties and fitting procedure

The main disadvantage of using the MAID PWA is that uncertainties are not provided. We thus assign a relative 5% error to every multipole, which is a common approach (see, e.g., Ref. [97] for a similar procedure in the analysis of pion-nucleon elastic scattering), such that the uncertainty of the observables reads for our case

$$\delta O_i = \sqrt{\left(0.05\, O_i^{\text{expt}}\right)^2 + \left(\delta O_i^{(n)}\right)^2} \tag{55}$$

with O_i^{expt} the given value of the observable and $\delta O_i^{(n)}$ the truncation error at order n. To estimate the uncertainties originating from the truncation of the chiral expansion we follow the Bayesian approach described in Ref. [1], which is based on the previous developments in the literature (see Refs. [64–66]). Below, we reproduce the main ingredients of this procedure.

We assume the following expansion with dimensionless coefficients c_i for an analyzed observable $\mathcal{O}$:

$$\begin{aligned}\mathcal{O} &= \mathcal{O}^{(1)} + \Delta\mathcal{O}^{(2)} + \Delta\mathcal{O}^{(3)} + \cdots \\ &= \mathcal{O}_{\text{ref}}\,(c_1 Q + c_2 Q^2 + c_3 Q^3 + \cdots),\end{aligned} \tag{56}$$

where $\Delta\mathcal{O}^{(i)} = \mathcal{O}^{(i)} - \mathcal{O}^{(i-1)}$ and the superscript i stands for the order in the small-scale expansion. As compared to Ref. [1], we adopt a definition more appropriate in the various considered energy regions of the small parameter Q, following Ref. [66]:

$$Q = \max\left(\frac{E_\pi}{\Lambda_b}, \frac{M_\pi^{\text{eff}}}{\Lambda_b}\right), \tag{57}$$

with $M_\pi^{\text{eff}} = 200$ MeV, instead of $Q = E_\pi/\Lambda_b$. The reference value $\mathcal{O}_{\text{ref}}$ is chosen to be

$$\mathcal{O}_{\text{ref}} = \max\left(\frac{|\mathcal{O}^{(1)}|}{Q}, \frac{|\Delta\mathcal{O}^{(2)}|}{Q^2}, \frac{|\Delta\mathcal{O}^{(3)}|}{Q^3}\right). \tag{58}$$

The coefficient c_m, where m is the number of a maximal argument in the max function in Eq. (58), defines the overall scale, $c_m = 1$, whereas the remaining coefficients are assumed to be distributed according to the Gaussian prior $\text{pr}(c_i|\bar{c})$:

$$\text{pr}(c_i|\bar{c}) = \frac{1}{\sqrt{2\pi}\,\bar{c}}\, e^{-c_i^2/(2\bar{c}^2)}. \tag{59}$$

The parameter $\bar{c}$ is assumed to obey a log-uniform probability distribution

$$\text{pr}(\bar{c}) = \frac{1}{\ln(\bar{c}_>/\bar{c}_<)}\,\frac{1}{\bar{c}}\,\theta(\bar{c}-\bar{c}_<)\,\theta(\bar{c}_>-\bar{c}), \tag{60}$$

with the cutoffs $\bar{c}_< = 0.5$, $\bar{c}_> = 10$ reflecting the naturalness assumption.

The truncation error $\delta\mathcal{O}^{(k)}$ is determined by the probability distribution $\text{pr}_h^C(\Delta)$ of the dimensionless quantity

$$\Delta_k = \sum_{n=k+1}^{\infty} c_n Q^n \approx \sum_{n=k+1}^{k+h} c_n Q^n, \tag{61}$$

where we choose $h = 10$. The 1σ error corresponds to the confidence level 0.68.

We have checked that the choice of the relative "experimental" error has negligible effects on the fit result by varying its size between 2% and 15%. Of course, our choice affects the fit quality, but we found that these effects are relatively small, because the uncertainties are dominated by the Bayesian truncation errors. To obtain the central values of the fit parameters, we minimize the χ^2 function,

$$\chi^2 = \sum_i \left(\frac{O_i^{\text{expt}} - O_i^{(n)}}{\delta O_i}\right)^2, \tag{62}$$

where the sum runs over all energy points from every multipole we incorporate in the configuration.

After obtaining the central values of the fit parameters, the corresponding uncertainties are determined from the covariance matrix, which is approximated by the inverse of the Hessian:

$$\begin{aligned}&\delta y_i = \sqrt{\text{Cov}(y_i, y_i)}, \quad \text{Cov}(y_i, y_j) = H_{ij}^{-1}, \\ &H_{ij} = \frac{1}{2}\frac{\partial^2\chi^2}{\partial y_i \partial y_j}\bigg|_{\boldsymbol{y}=\bar{\boldsymbol{y}}}.\end{aligned} \tag{63}$$

Here, the vector $\boldsymbol{y}$ refers to the set of all fitting parameters, and $\bar{\boldsymbol{y}}$ is the vector of best fit values.

2. Energy range

The energy range in which χPT is applicable is limited by the lowest-lying not included resonance, which is in the Δ-less formulation the Δ particle. Thus, the Δ energy region should be excluded completely in the Δ-less fit, so that we choose to restrict the upper energy boundary to $\sqrt{s} = 1200\,\text{MeV}$. By construction, we expect the range of convergence of HBχPT to be smaller than in the covariant case. Also, in previous studies, it was shown that the HB approach yields good agreement with the neutral pion production data only up to 20 MeV above threshold [98]. Furthermore, we exclude the region very close to the pion production threshold. Since we work in the isospin-symmetric limit, which leads to equal pion masses, our calculation cannot account for effects generated by the mass difference of the pions. The reaction threshold lies at $\sqrt{s} \approx 1076\,\text{MeV}$, so we restrict the lower energy boundary of our fits to $\sqrt{s} = 1090\,\text{MeV}$. We choose energy steps of 2 MeV, so we have 56 data points per observable in the Δ-less case. Briefly stated, we use the energy range $1090 \leqslant \sqrt{s} \leqslant 1200$ MeV in the Δ-less fit.

In the Δ-full case, we extend the upper energy boundary to $\sqrt{s} = 1250\,\text{MeV}$ to partially take into account the Δ region. By construction of the complex-mass approach, unitarity is strongly violated very close to threshold due to the constant imaginary part of the Δ mass in the Δ pole diagrams. However, unitarity will be restored perturbatively when including higher orders. As long as we first include only the Δ tree diagrams, we expect the description of the data to be worse near threshold compared to the Δ-less approach. However, these effects should be dominant in the imaginary parts of the multipoles, which we do not fit. Therefore, we still choose to include the threshold region in our fitting range and comment on the description of the threshold region in the next section. Stated briefly, we fit in the range $1090 \leqslant \sqrt{s} \leqslant 1250$ MeV.

In our ϵ^3 study, we have again modified the energy range. In principle, the same arguments as in the case of $Q^3 + \epsilon^2$ hold, but we found that the data in the threshold region significantly affect the subleading $\gamma N\Delta$ coupling constant h_1, while having little impact on the other LECs. Because we are interested in a precise determination of the $\gamma N\Delta$ couplings, we removed the threshold region in the ϵ^3 fits and take into account only the data for the range $1150 \leqslant \sqrt{s} \leqslant 1250$ MeV.

3. Data configuration

We restrict ourselves to the analysis of s- and p-wave multipoles, because they contain by far the largest contributions to the photoproduction cross sections. Moreover, in higher partial waves, the unknown LECs contribute only as $1/m_N$ corrections. In Fig. 1, the results of the MAID analysis are depicted [95]. Furthermore, the results of the energy-dependent [99,100] and energy-independent [101] GWU-SAID multipole amplitudes are shown in order to illustrate differences between various partial-wave analyses. The agreement between the three sets of data is excellent for the $M_{1+}^{3/2}$ multipole, which corresponds to the magnetic excitation of the Δ resonance in the s channel, and reasonably good for the E_{0+} and M_{1-} multipoles.

In the Δ-less case, we are interested in choosing a fit configuration sensitive to the values of the LECs d_8, d_9, d_{20}, and $d_{21;22}$. Therefore, it is instructive to analyze the contributions of the parameters to the various amplitudes. The three multipoles E_{0+}, M_{1+}, and M_{1-} all receive leading-order contributions of one or several LECs with respect to the $1/m_N$ expansion, i.e., $\mathcal{O}(m_N^0)$. The multipole E_{1+} gets only next-to-leading-order $1/m_N$ contributions from all four parameters; therefore, we exclude E_{1+} completely from the Δ-less fit. We choose to fit the $I = 3/2$ channel first, which is motivated by the agreement of the data sets, the order of magnitude of the multipoles, and bearing in mind that we are interested in analyzing the differences to the Δ-full theory, which is expected to bring dominant contributions to the $I = 3/2$ channel. Altogether, we first fit to the three multipole amplitudes $E_{0+}^{3/2}$, $M_{1+}^{3/2}$, and $M_{1-}^{3/2}$, which determines the parameters d_8, d_{20}, and $d_{21;22}$. The constant d_9 does not contribute to the $I = 3/2$ channel and is fitted to the $I = 1/2$ channels subsequently. We anticipate that the constants d_8, d_{20}, and $d_{21;22}$ are sufficiently constrained from the $I = 3/2$ fit to serve as an input for the $I = 1/2$ fit. At leading order in $1/m_N$, d_9 contributes to both proton and neutron channels of $M_{1+}^{1/2}$ and $M_{1-}^{1/2}$. However, while performing the fit, we found that there is no value of d_9 which results in an acceptable description of $M_{1-}^{1/2}$. This is caused by large loop contributions to these multipoles. We expect that this problem is resolved if higher-order contributions are taken into account. Thus, we decided to exclude $M_{1-}^{1/2}$ from the second fit and determine d_9 only from $M_{1+}^{1/2}$. When removing M_{1-}, the central value of d_9 only changes very slightly, which supports our strategy, but of course the fit quality is affected. The uncertainty of d_9 is determined analogously to Eq. (63) by

$$\delta d_9 = \left(\frac{1}{2} \frac{\partial^2 \chi^2_{I=1/2}}{\partial d_9^2} \right)^{1/2} . \tag{64}$$

This procedure neglects the fact that δd_9 also receives contributions from the uncertainties of the previously determined LECs. We have checked that these effects indeed have a small impact, so that it is legitimate to ignore them. This insight also supports our idea that d_8, d_{20}, and $d_{21;22}$ are sufficiently well constrained by the first fit.

In the case of including the Δ-full ϵ^2 tree diagrams, the additional constant b_1 is introduced. In the s channel, b_1 contributes at leading order in $1/m_N$ only to M_{1+}, which is already part of our fitting configuration. As b_1 contributes to the $I = 3/2$ channel, we obtain its central value as well as $\bar{d}_8$, $\bar{d}_{20}$, and $\bar{d}_{21;22}$ from the $I = 3/2$ fit. Subsequently, we determine $\bar{d}_9$ from the $I = 1/2$ channel as before. Note that at this working order, it is not necessary to distinguish between covariant or HB b_1, because $1/m_N$ corrections and renormalization counterterms are beyond the working order.

At order ϵ^3, one includes the leading Δ-full loops and the tree diagrams with the additional constant $\bar{h}_1$. The s-channel Δ-pole graphs with $\bar{h}_1$ give essential contributions to the electric Δ multipole E_{1+}. Therefore, we slightly modify our fitting procedure and include E_{1+} in the $I = 3/2$ fit, which determines in the following the covariant LECs $\bar{d}_8$, $\bar{d}_{20}$, $\bar{d}_{21;22}$,

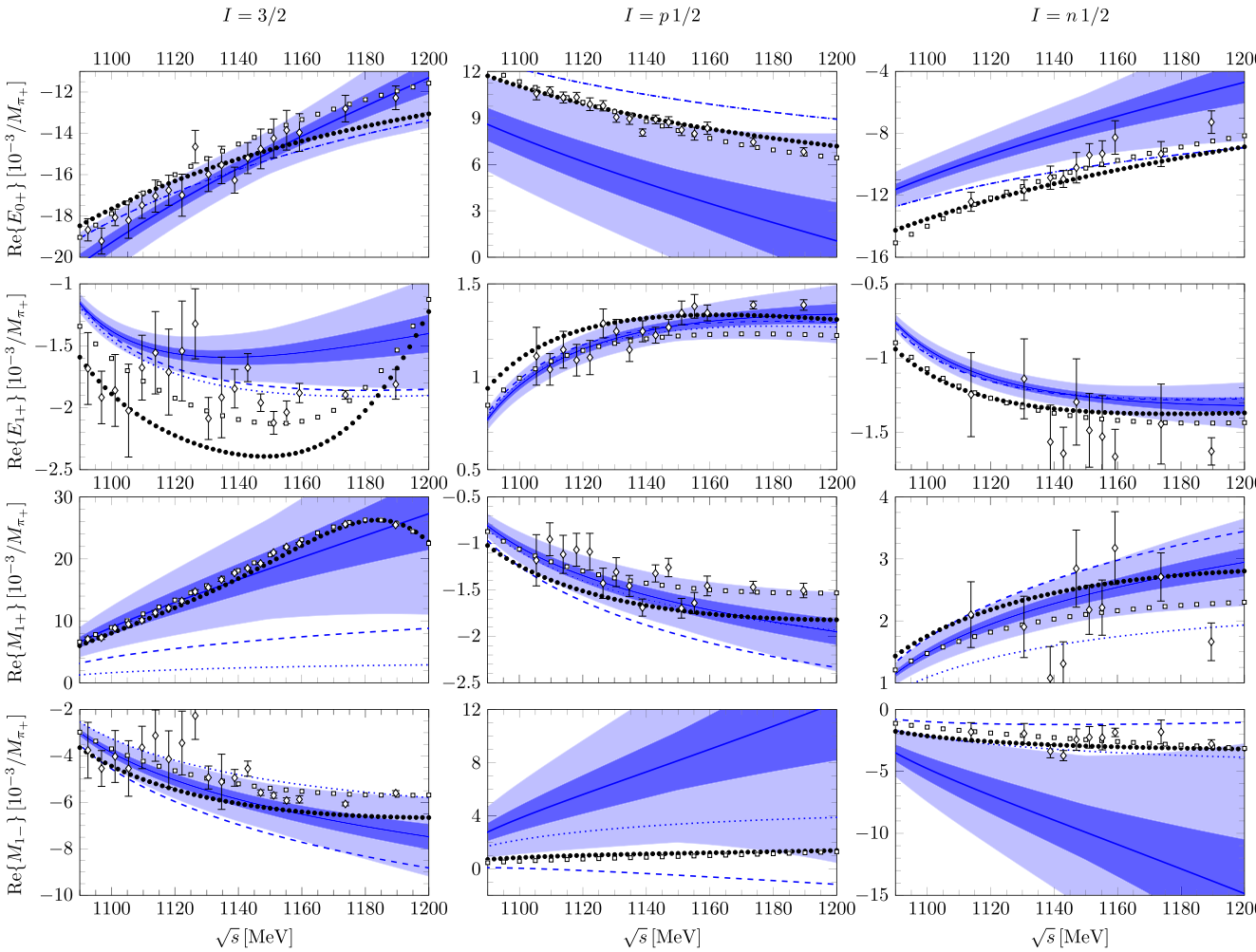

FIG. 1. Order-Q^3 fits obtained in the heavy-baryon approach to the real parts of the s- and p-wave photoproduction multipoles. The solid, dashed, and dotted lines denote the Q^3, Q^2, and Q^1 results, respectively. The darker (lighter) shaded bands show the estimated truncation errors at order Q^3 with 1σ (2σ) confidence. The solid circles show the results of the MAID PWA from Ref. [95], and the squares (diamonds) are the results of the energy-dependent (energy-independent) SAID analysis from Refs. [99,100] (Ref. [101]).

$\bar{b}_1$, and $\bar{h}_1$. Subsequently, we fit $\bar{d}_9$ to the $I = 1/2$ channel as before. At this working order, we find it to be especially important to consider $I = 3/2$ separately in order to access $\bar{h}_1$. Because $\bar{h}_1$ starts to contribute from one order higher in the $1/m_N$ series, we assume that our fits are rather insensitive to this constant. The relation between the bare LEC h_1 and the renormalized LEC $\bar{h}_1$ was given in Sec. IV (the same applies to b_1 and $\bar{b}_1$).

Note that in the studies based on the δ counting (e.g., in Refs. [59–62,102]), a different convention for the $\gamma N\Delta$ structures in the effective Lagrangian is adopted in terms of the constants g_M and g_E. The on-shell matching leads to the following relation among the two sets of constants [1]:

$$\bar{b}_1 = 3\frac{m_\Delta}{m_N(m_N+m_\Delta)}g_M, \quad \bar{h}_1 = \frac{3}{2}\frac{1}{m_N+m_\Delta}(g_E+g_M). \tag{65}$$

Nevertheless, a direct comparison of the numerical values of the $\gamma N\Delta$ constants obtained in different schemes would be misleading because they are not observable. A better strategy is to compare with empirical quantities, such as the ratio of the electric and magnetic Δ multipoles in the Δ region as we do below.

C. Order Q^3 results

In Table II, we show our fit results for the HB LECs including uncertainties. For the $I = 3/2$ ($I = 1/2$) fit, we used 168 (112) data points, so that the reduced χ^2/n is equal to 0.9

TABLE II. Low-energy constants obtained from a Δ-less order-Q^3 fit in the HB approach to the real parts of s- and p-wave photoproduction multipoles of the MAID model from Ref. [95]. All LECs are given in units of GeV^{-2}.

	$\hat{d}_8^r$	$\hat{d}_9^r$	$\hat{d}_{20}^r$	$\hat{d}_{21;22}^r$
HB order-Q^3 fit value	−7.7(3)	0.03(2)	−17.2(5)	14.3(5)

TABLE III. Low-energy constants obtained from a Δ-less order-Q^3 covariant fit to the real parts of s- and p-wave photoproduction multipoles of the MAID model from Ref. [95]. All LECs are given in units of GeV^{-2}.

	$\bar{d}_8$	$\bar{d}_9$	$\bar{d}_{20}$	$\bar{d}_{21;22}$
Covariant order-Q^3 fit value	−4.9(2)	0.01(1)	−8.5(3)	9.4(4)

(1.8), where n stands for the number of data points minus the number of fitted LECs. Table III collects the corresponding results of the covariant approach, where we emphasize again that the fits are fully comparable in terms of data configuration and energy range. In the covariant formalism, we obtain for the reduced χ^2/n 0.3 (0.2) for the $I = 3/2$ ($I = 1/2$) fit.

The HB (covariant) fit results are shown in Figs. 1 (2), respectively, where the plotted energy range corresponds to our fitting range. At this point, we remind that in the $I = 3/2$ channel, $E_{1+}^{3/2}$ has not been used in the fit. In both $I = 1/2$ channels, only $M_{1+}^{1/2}$ was used for the fit; all other multipoles are predictions. We also remind that we used the 1σ confidence interval for the determination of the truncation errors, but our figures also show the 2σ band. Also, we adopted a rather conservative value of the breakdown scale of the chiral expansion $\Lambda_b = 650\,\text{MeV}$ motivated by recent studies in the few-nucleon sector [66,103]. Notice, however, that this estimation of Λ_b in the few-nucleon sector [64,103,104] does not necessarily apply to the case at hand. In particular, for reactions where the Δ resonance plays an important role, e.g., pion-nucleon scattering at intermediate energies, the breakdown scale of the Δ-less χPT is considerably lower (see, e.g., Ref. [67]).

In the $I = 3/2$ channel, we find both HB and covariant descriptions satisfactory with the exception of the electric Δ multipole $E_{1+}^{3/2}$, which is not well reproduced. The latter fact is probably due to the missing Δ contributions. We expect the description of this amplitude to improve when including them, which will be discussed in Sec. V D. Note that the shape of the $M_{1+}^{3/2}$ multipole is not well reproduced for c.m. energies above $\sqrt{s} = 1150\,\text{MeV}$, which is also due to missing Δ dynamics. We expect that the inclusion of the Δ contributions will correct this behavior significantly (see also Sec. V D). The $E_{0+}^{3/2}$ and $M_{1-}^{3/2}$ multipoles are better described in the covariant

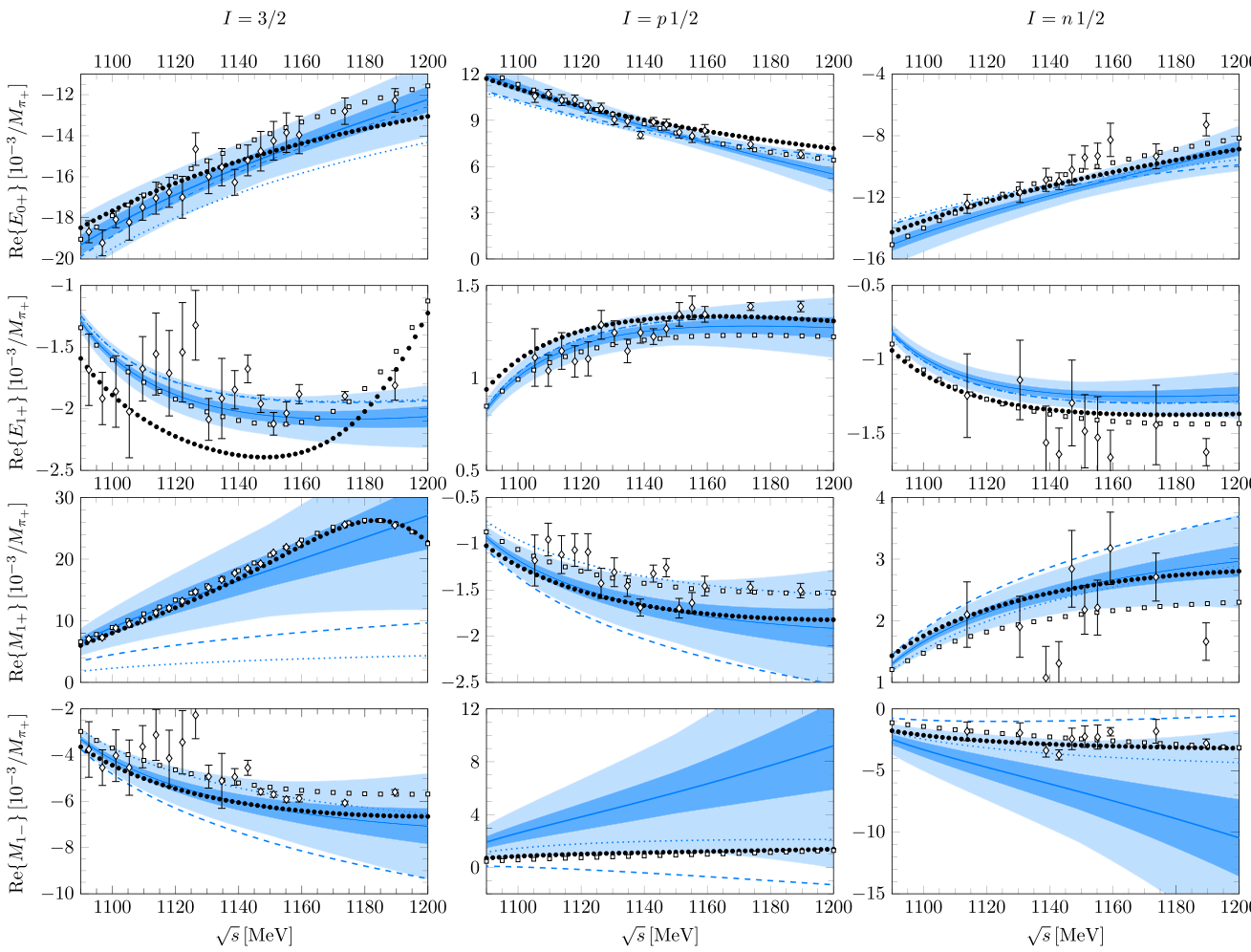

FIG. 2. Order-Q^3 fits obtained in the covariant approach to the real parts of the s- and p-wave photoproduction multipoles. The notation is as in Fig. 1.

TABLE IV. Low-energy constants obtained from an order-$(Q^3+\epsilon^2)$ covariant fit to the real parts of s- and p-wave photoproduction multipoles of the MAID model from Ref. [95]. All LECs are given in units of GeV^{-2}; b_1 is given in m_N^{-1}.

	$\bar{d}_8$	$\bar{d}_9$	$\bar{d}_{20}$	$\bar{d}_{21;22}$	b_1
Covariant order-$(Q^3+\epsilon^2)$ fit value	0.72(3)	0.02(1)	−2.1(1)	−0.1(1)	5.6(1)

case, which explains the differences in the fit quality. The smaller value of χ^2/n in the covariant approach may indicate that the Bayesian truncation uncertainties are overestimated or that the fit range is not broad enough to constrain the LECs sufficiently. At this point we emphasize that n should not be equated with the number of degrees of freedom, because our choice of the number of data points is in some way arbitrary. Varying the energy steps results in different values of the reduced χ^2/n; therefore, one cannot associate a perfect fit with a value of $\chi^2/n=1$. The values of χ^2/n should, therefore, not be directly interpreted as a statistical measure of the fit quality but used to compare the relative quality of fits obtained with the same preconditions. Generally, one expects the values of the multipoles at neighboring energy points to be correlated, so that the actual number of degrees of freedom is presumably much smaller than n. Moreover, we also neglect possible correlations among the theoretical errors at different energies, which makes our error estimates more conservative. For a detailed discussion of the effects of such correlations, we refer the reader to Ref. [105]. For these reasons, good fits of the empirical data are expected to have χ^2/n considerably smaller than 1.

In the $I=1/2$ channels, the difference between HB and covariant approaches is more pronounced. The description of $E_{0+}^{1/2}$ of the MAID analysis is clearly better in the covariant approach, and also the description of $M_{1+}^{1/2}$ is better, which is reflected in the fit quality. Clearly, the value of $\chi^2/n=1.8$ in the HB case shows that the data cannot be well described. On the other hand, the small value of $\chi^2/n=0.2$ obtained in the covariant approach indicates that more data might be required to constrain d_9 better.

With the obtained fit values in both approaches, we now analyze the numerical differences between HB and covariant constants as discussed in Sec. V A. Substituting the employed values of g_A and F_π into the right-hand sides of Eqs. (53), the numerical values of the predicted shifts read

$$\Delta d_8^{\mathrm{IR}}=0.6\,\mathrm{GeV}^{-2},\qquad \Delta d_9^{\mathrm{IR}}=0.08\,\mathrm{GeV}^{-2},$$
$$\Delta d_{20}^{\mathrm{IR}}=2.8\,/\,\mathrm{GeV}^{2},\qquad \Delta d_{21;22}^{\mathrm{IR}}=-1.9\,\mathrm{GeV}^{-2}, \tag{66}$$

whereas we find for the actual differences from Tables II and III

$$\bar{d}_8-\hat{d}_8^r=2.8\,\mathrm{GeV}^{-2},\qquad \bar{d}_9-\hat{d}_9^r=-0.02\,\mathrm{GeV}^{-2},$$
$$\bar{d}_{20}-\hat{d}_{20}^r=8.7\,\mathrm{GeV}^{-2},\qquad \bar{d}_{21;22}-\hat{d}_{21;22}^r=-4.9\,\mathrm{GeV}^{-2}. \tag{67}$$

These results show that the IR shifts can, at best, only qualitatively explain the differences between HB and covariant approaches. In particular, the agreement for d_9 is excellent, while for d_8, d_{20}, and $d_{21;22}$, the differences have the same sign as the IR shift. The remaining gap between the two sets of fit parameters is probably due to the poorer fit quality in the HB approach. We also find that the values of the covariant LECs are more natural as in the HB approach. Here, the term "natural" refers to the naive estimate that the d_i's should roughly be of order 1 in the units of Λ_b^{-2}:

$$d_i\sim\frac{1}{\Lambda_b^2}\approx 2.5\ \mathrm{GeV}^{-2}\ \text{with}\ \Lambda_b=650\ \mathrm{MeV}. \tag{68}$$

D. Order-$(Q^3+\epsilon^2)$ results

In Table IV, we show our fit results for the LECs in the covariant approach at order $Q^3+\epsilon^2$. The reduced χ^2/n is equal to 0.5 (1.0) in the $I=3/2$ ($I=1/2$) channel.

In Fig. 3, we show the results. The most outstanding difference from the Δ-less case is the significantly improved description of the $M_{1+}^{3/2}$ multipole. In comparison to the Δ-less approach, the region beyond $\sqrt{s}=1150\,\mathrm{MeV}$ is reproduced excellently both in magnitude and in shape. The leading Δ tree diagrams suffice to correct the Q^3 description of $M_{1+}^{3/2}$. However, the description of $E_{1+}^{3/2}$ is unsatisfactory. We presume that including ϵ^3 terms will improve the description, because the subleading $\gamma N\Delta$ coupling constant h_1 contributes at its leading order in $1/m_N$ to $E_{1+}^{3/2}$. In the $I=1/2$ channels, for all s and p waves, the data description is not worse than in the Δ-less case. Only $M_{1+}^{1/2}$ was fitted for comparability with the Δ-less approach; all other multipoles are reproduced to a good extent. Here, $M_{1-}^{1/2}$ must be accentuated, which was overshot dramatically in the Δ-less theory.

For the sake of completeness, we mention that we also performed fully comparable fits in the HB approach, using a consistent value of the Δ mass fitted to the HB order-ϵ^2 amplitude of $m_\Delta=(1196.1-45.2\,\mathrm{i})\,\mathrm{MeV}$. In Fig. 4, we show E_{0+} and M_{1+} in the $I=1/2$ channel in order to illustrate that the HB results are, however, by far not as satisfying as the covariant results, which we observe for all multipoles. We conclude that, as expected, the heavy-baryon (nonrelativistic) expansion is not quite efficient if one wants to extend the scheme to the Δ region. Therefore, we do not give the full set of results here; however, we found that the resulting value of $b_1=5.5(1)m_N^{-1}$ is still very close to the covariant one. This is a nice indication of the stability of this constant.

Next, we take a look at the differences between the Δ-less and Δ-full fit values of the LECs from the point of Δ resonance saturation, as explained in Sec. V A. Numerically, the expected differences read, using the covariant fit value of b_1,

$$\delta d_8(\Delta)=-\delta d_{21;22}(\Delta)=-3.4\,\mathrm{GeV}^{-2}, \tag{69}$$

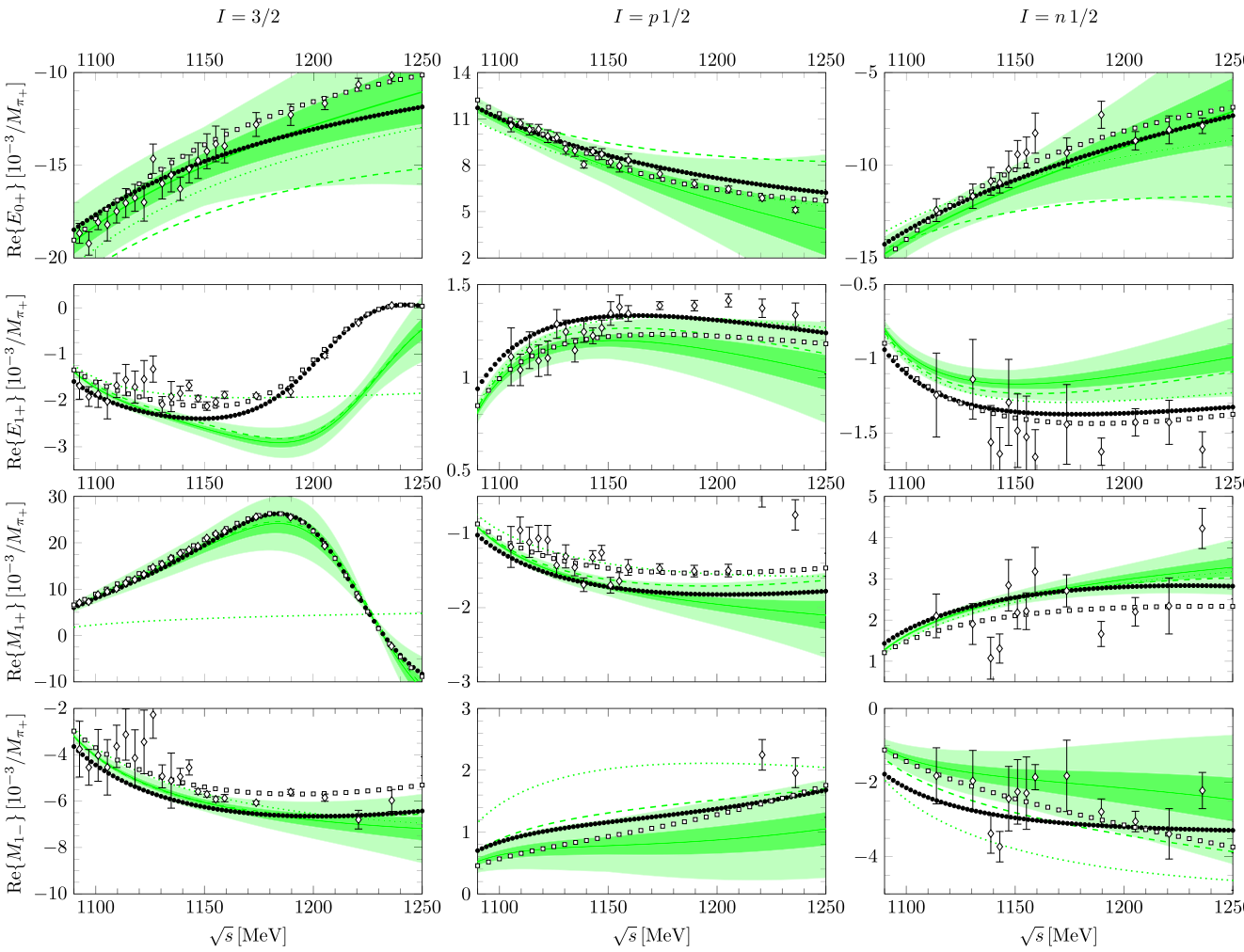

FIG. 3. Order-$(Q^3+\epsilon^2)$ fits obtained in the covariant approach to the real parts of the s- and p-wave photoproduction multipoles. The solid, dashed, and dotted lines denote the $Q^3+\epsilon^2$, ϵ^2, and ϵ^1 results, respectively. The darker (lighter) shaded bands show the estimated truncation errors at order Q^3 with 1σ (2σ) confidence. The solid circles show the results of the MAID PWA from Ref. [95], and the squares (diamonds) are the results of the energy-dependent (energy-independent) SAID analysis from Refs. [99,100] (Ref. [101]).

and for the actual differences

$$\bar{d}_8^{\not\Delta} - \bar{d}_8^{\Delta} = -5.6\,\mathrm{GeV}^{-2}, \qquad \bar{d}_9^{\not\Delta} - \bar{d}_9^{\Delta} = -0.01\,\mathrm{GeV}^{-2},$$
$$\bar{d}_{20}^{\not\Delta} - \bar{d}_{20}^{\Delta} = -6.4\,\mathrm{GeV}^{-2}, \qquad \bar{d}_{21;22}^{\not\Delta} - \bar{d}_{21;22}^{\Delta} = 9.5\,\mathrm{GeV}^{-2}. \tag{70}$$

As one can see, the differences between Δ-less and Δ-full parameters are only very qualitatively explained by the resonance saturation.

In the following, we compare our covariant order-$(Q^3+\epsilon^2)$ results with data of the neutral pion production channel $\gamma p \to \pi^0 p$. Of the four physical reaction channels given in Eq. (8), this channel is the most interesting for our purposes. The amplitudes for the two charged pion production channels $\gamma p \to \pi^+ n$ and $\gamma n \to \pi^- p$ are dominated by the leading-order Kroll-Ruderman terms, such that subleading terms give only very small corrections. The remaining neutral channel $\gamma n \to \pi^0 n$ is difficult to measure in experiments since this requires a neutron target. Therefore, little data are available for this channel.

The recent experiment at the Mainz Microtron (MAMI) provided high-precision data for the differential cross section $\frac{\mathrm{d}\sigma}{\mathrm{d}\Omega}$ and the linearly polarized photon asymmetry Σ [38,39,70]. We compare our findings with these data and emphasize that our results for both observables were calculated as discussed in Sec. II; in particular we do not use the s- and p-wave approximation. In Figs. 5 and 6, we depict our results obtained from the covariant order-$(Q^3+\epsilon^2)$ fit, where the depicted error bars show the combined statistical and systematic error:

$$\delta O_i = \sqrt{\left(\delta O_i^{\mathrm{stat}}\right)^2 + \left(\delta O_i^{\mathrm{sys}}\right)^2}. \tag{71}$$

The systematic uncertainties are 4% for $\frac{\mathrm{d}\sigma}{\mathrm{d}\Omega}$ and 5% for Σ.

In the analysis of the s- and p-wave multipole amplitudes, we found that the order-$(Q^3+\epsilon^2)$ covariant fits give an overall accurate reproduction in our considered energy region. By comparison with the differential cross section and polarization asymmetry, we find our observation confirmed. Both

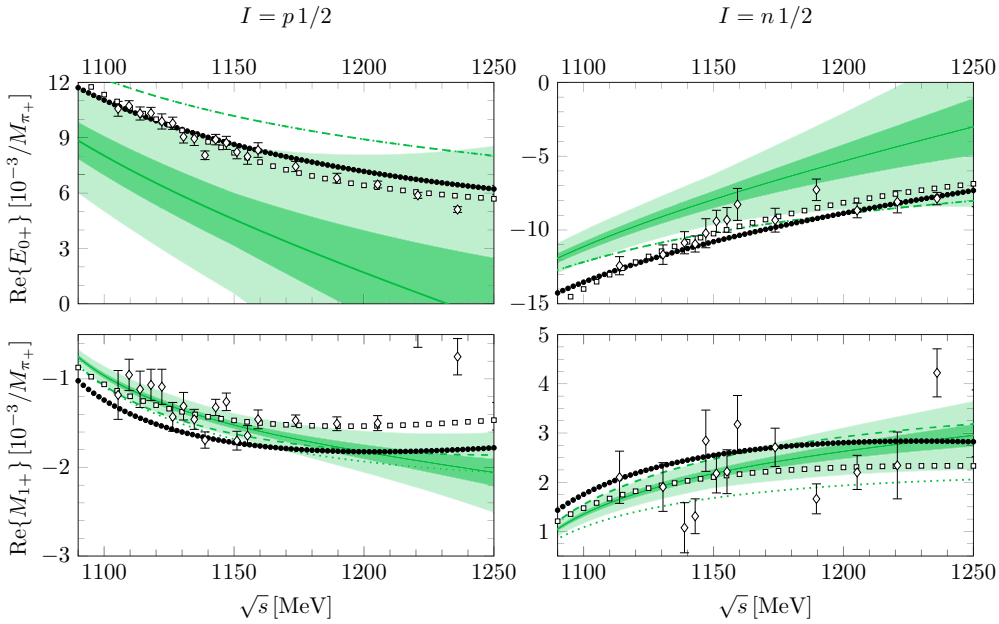

FIG. 4. Selected plots of order-$(Q^3+\epsilon^2)$ fits obtained in the heavy-baryon approach to the real parts of the s- and p-wave photoproduction multipoles. The notation is as in Fig. 3.

observables are reproduced rather accurately up to the Δ region as expected from the quality of the fit to the multipoles. The apparent underestimation of the theoretical errors for some energies is due to a worse convergence of the chiral expansion for the neutral channels. In particular, the order-Q^1 contribution is absent in these channels, which makes the number of considered orders insufficient for a reliable truncation error estimation in the Bayesian approach.

E. Order ϵ^3 results

Finally, we give our results for the LECs determined from the covariant fit at order ϵ^3 in Table V. In the $I = 3/2$ fit, the number of used data points is 204 due to the inclusion of the E_{1+} multipole and 102 in the $I = 1/2$ channel. The reduced χ^2/n is equal to 0.2 (2.2) in the $I = 3/2$ ($I = 1/2$) channel. The corresponding results for the multipoles are depicted in Fig. 7. As we can see from Fig. 7, the reproduction of the $I = 3/2$ channel has improved compared to the covariant

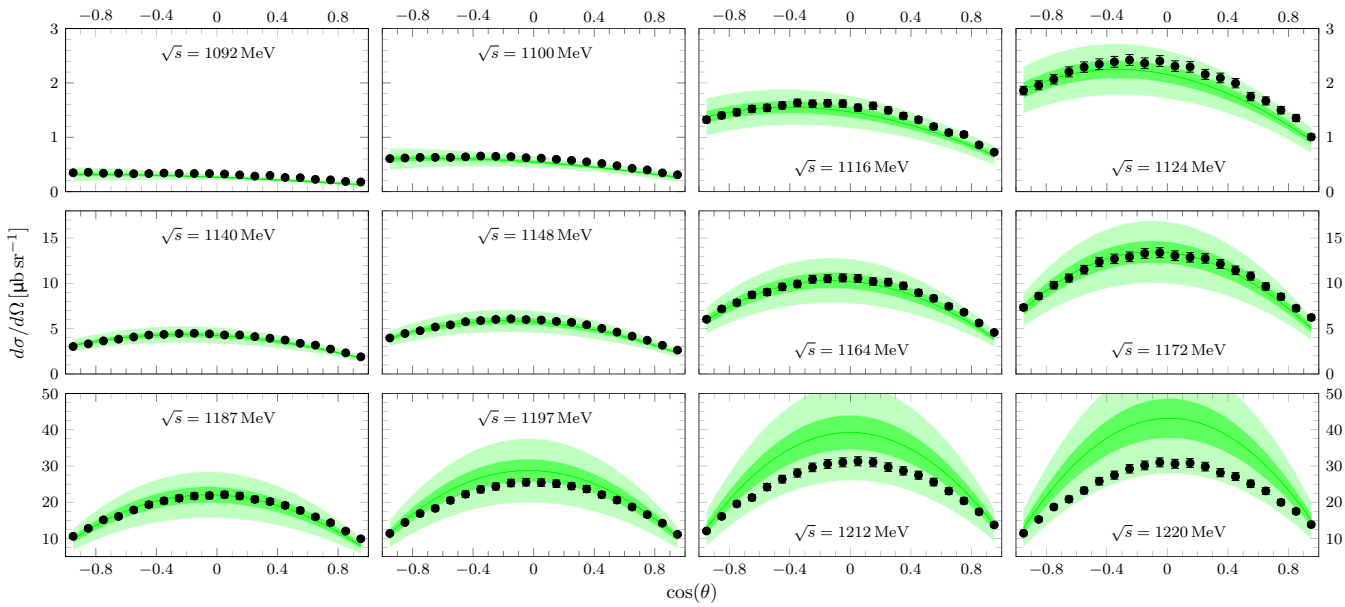

FIG. 5. Covariant order-$(Q^3+\epsilon^2)$ result of the unpolarized differential cross section in the channel $\gamma + p \to \pi^0 + p$. The solid lines denote the $Q^3+\epsilon^2$ results, and the darker (lighter) shaded bands show the estimated truncation errors at order $Q^3+\epsilon^2$ with 1σ (2σ) confidence. The data are from Refs. [38,70]; error bars correspond to the combined statistical and systematical error.

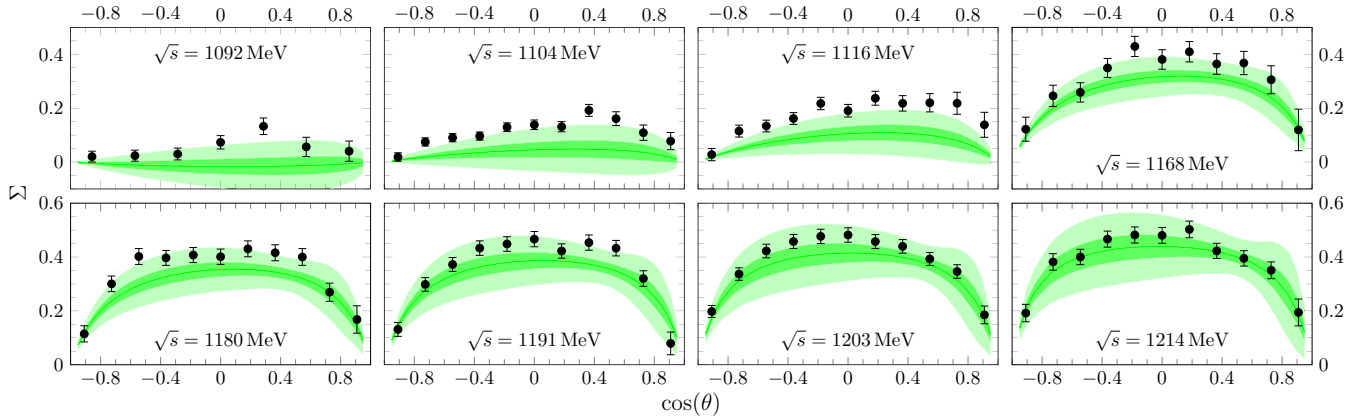

FIG. 6. Covariant order-$(Q^3+\epsilon^2)$ result of the linearly polarized photon asymmetry in the channel $\gamma + p \to \pi^0 + p$. The solid lines denote the $Q^3+\epsilon^2$ results, and the darker (lighter) shaded bands show the estimated truncation errors at order $Q^3+\epsilon^2$ with 1σ (2σ) confidence. The data are from Refs. [38,39,70]; error bars correspond to the combined statistical and systematical error.

$Q^3+\epsilon^2$ fit. In particular, E_{1+} is now matched significantly better due to the inclusion of the subleading $\gamma N\Delta$ coupling constant $\bar{h}_1$. In the $I=1/2$ channels, however, the description is distinctly worse compared to the $Q^3+\epsilon^2$ case. In particular, the reproduction of the $E_{0+}^{1/2}$ multipoles fails, which has a substantial effect on the reproduction of cross sections, for example. Also, the fit quality in the $I=1/2$ channels of $\chi^2/n = 2.2$ is significantly worse compared to the $Q^3+\epsilon^2$ fit, where we found $\chi^2/n = 1.0$. We also remark that $M_{1-}^{1/2}$ is overshot again, but not as badly as in the Δ-less case (see Fig. 2). These observations indicate a slow convergence of the scheme in the $I=1/2$ channels, and one needs to extend the calculation to higher orders (such as $Q^4+\epsilon^3$ or ϵ^4) to obtain a better description of the data.

To check that our determined value of the Δ mass in the covariant scheme is consistent with the Δ contribution to the πN elastic channel, we plot the imaginary part of $E_{1+}^{3/2}$ and $M_{1+}^{3/2}$ in Fig. 8. Because the phase of the pion photoproduction amplitude is determined by the elastic πN phase shifts, a satisfying reproduction of the imaginary parts is important. We find the agreement reasonable, with the deviation in $\mathrm{Im}\{M_{1+}^{3/2}\}$ close to threshold originating from the usage of the constant imaginary part of the Δ mass in the Δ-pole diagrams. Furthermore, the $E2/M1$ ratio

$$R_{EM} = \left.\frac{\mathrm{Im}\{E_{1+}^{3/2}\}}{\mathrm{Im}\{M_{1+}^{3/2}\}}\right|_{\sqrt{s}=1232\,\mathrm{MeV}} \approx -0.033 \pm 0.014 \qquad (72)$$

is consistent with the PDG value $-0.030 \lesssim R_{EM} \lesssim -0.020$ [91], whereas at order $Q^3+\epsilon^2$, we found $R_{EM} \approx -0.071 \pm 0.014$.

Finally, to analyze the efficiency of the SSE and the δ expansion, we have compared the terms in the amplitude proportional to $h_A^2 g_A$ and to $h_A^2 g_1$. The former contribution is generated by one-loop diagrams with one and two Δ lines, whereas the latter one originates from one-loop graphs with two and three Δ lines. While this is not exactly the separation encountered in the δ expansion, these two types of contributions are individually gauge invariant as explained in Sec. III, which makes their comparison model independent.

It turns out that the $h_A^2 g_1$ terms are typically smaller than the $h_A^2 g_A$ terms. Their maximal contribution (relative to the $h_A^2 g_A$ terms) is observed in the multipoles M_{1+} and M_{1-} for all isospin channels and amounts to 30–50%. This ratio is consistent with the expectations based on the δ counting, namely, $\delta = M_\pi/\Delta \approx 0.5$. However, the description of the data in the $I=1/2$ channel is worse at order ϵ^3 than at order $Q^3+\epsilon^2$, which might be an indication that some higher-order contributions are important. Therefore, the comparison seems rather inconclusive at this point. To draw a clearer conclusion, it would be desirable to extend the scheme to higher orders and look at relative importance of terms of order $\mathcal{O}(Q^4)$ and $\mathcal{O}(\epsilon^4)$.

VI. SUMMARY AND CONCLUSIONS

We have studied pion photoproduction in chiral effective field theory with explicit Δ degrees of freedom. Starting from the Δ-less approach, we considered the reaction up to the leading loop order in the heavy-baryon and in the manifestly covariant schemes. In particular, we analyzed the difference between the obtained HB and covariant results for low-energy constants in terms of the infrared regular shifts. We extended

TABLE V. Low-energy constants obtained from an order-ϵ^3 covariant fit to the real parts of s- and p-wave photoproduction multipoles of the MAID model from Ref. [95]. All LECs are given in units of GeV^{-2}; $\bar{b}_1$ and $\bar{h}_1$ are given in m_N^{-1}.

	$\bar{d}_8$	$\bar{d}_9$	$\bar{d}_{20}$	$\bar{d}_{21;22}$	$\bar{b}_1$	$\bar{h}_1$
Covariant order-ϵ^3 fit value	−0.25(4)	−0.73(2)	2.2(1)	−6.8(1)	5.3(1)	0.9(1)

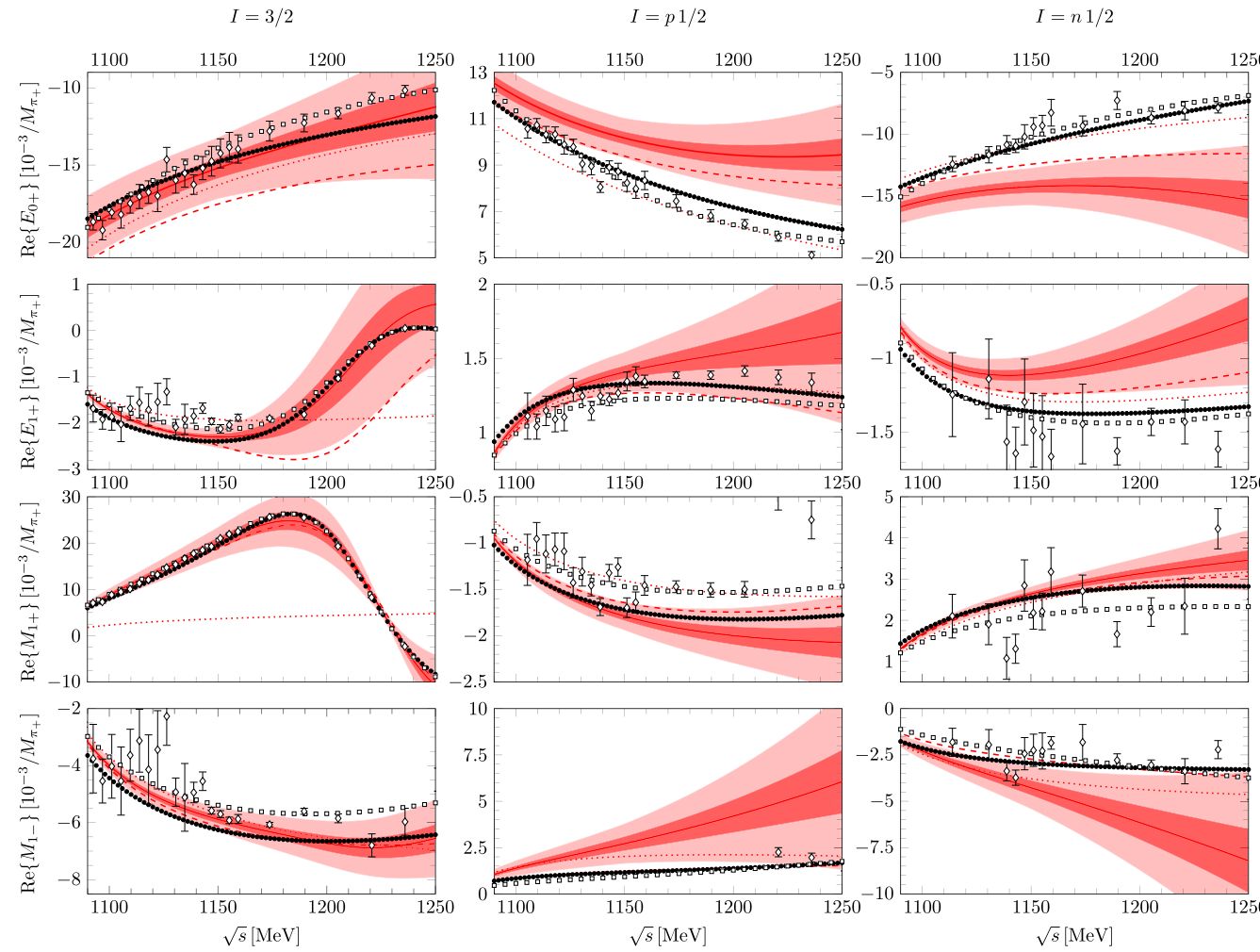

FIG. 7. Order-ϵ^3 fits obtained in the covariant approach to the real parts of the s- and p-wave photoproduction multipoles. The solid, dashed, and dotted lines denote the ϵ^3, ϵ^2, and ϵ^1 results, respectively. The darker (lighter) shaded bands show the estimated truncation errors at order Q^3 with 1σ (2σ) confidence. The solid circles show the results of the MAID PWA from Ref. [95]; the squares (diamonds) are the results of the energy-dependent (energy-independent) SAID analysis from Refs. [99,100] (Ref. [101]).

our calculations to the leading Δ contributions employing the complex-mass approach using a fitted Δ mass and studied the effects of resonance saturation to the LECs. Moreover, we for the first time provide results for pion photoproduction at order ϵ^3 in the small scale expansion scheme, where the leading Δ-full loop order is taken into account. The results for the LECs $\bar{d}_8$, $\bar{d}_9$, $\bar{d}_{20}$, $\bar{d}_{21;22}$, $\bar{b}_1$, and $\bar{h}_1$ are obtained by fits to

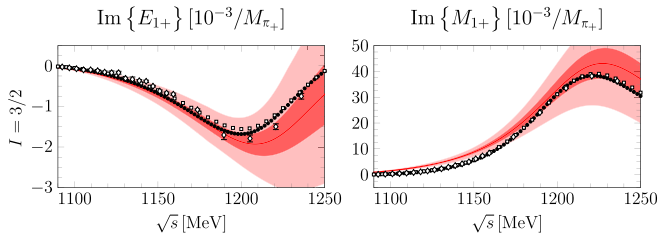

FIG. 8. Imaginary parts of $E_{1+}^{3/2}$ and $M_{1+}^{3/2}$ using the covariant order-ϵ^3 fit results. The notation is as in Fig. 7.

the MAID partial-wave analysis using a Bayesian approach to theoretical uncertainties.

The main conclusions of our analysis of pion photoproduction can be summarized as follows:

(i) In the Δ-less approach, the description of pion photoproduction is satisfying only in a very limited energy range above threshold and fails approaching the Δ region. Especially for the magnetic multipole $M_{1+}^{3/2}$, the description agrees with the data only up to approximately $\sqrt{s} = 1150\,\mathrm{MeV}$. Studying the reaction in the covariant framework yields a better agreement with the data than the heavy-baryon approach. The results of our calculations are very relevant for ongoing investigations of few-nucleon electromagnetic reactions (see Ref. [106] for a review article). While the two-nucleon charge density operator at the leading one-loop order does not involve LECs from $\mathcal{L}_{\pi N}^{(3)}$ [3,107], which allowed us to perform high-accuracy calculation of the deuteron charge and quadrupole

form factors [108,109], the corresponding current operator depends on the LECs d_8, d_9, d_{21}, and d_{22} [3]. In particular, the LEC d_9 governs the long-range two-nucleon contribution to the deuteron magnetic form factor [4].

(ii) Incorporating the leading Δ tree contributions significantly extends the energy range in which a good agreement with the s- and p-wave multipoles can be achieved. We found that the leading $\gamma N\Delta$ coupling constant b_1 is stable with respect to variation of the energy range, assigned relative error to the data, and combination of $I = 3/2$ and $I = 1/2$ fit. The difference between the numerical values of the LECs obtained in a Δ-less and Δ-full approach can, at least very qualitatively, be explained in terms of resonance saturation. The results from the covariant order-$(Q^3 + \epsilon^2)$ calculation are found to reproduce the high-precision data of cross sections and polarization asymmetries from Refs. [38,39,70] remarkably well. However, the order-$(Q^3 + \epsilon^2)$ calculation performed within the heavy-baryon scheme demonstrates a much worse description of the data. This is an indication of the fact that the $1/m_N$ expansion is not efficient in the Δ region.

(iii) The next-to-leading Δ contributions give rise to surprisingly large corrections to the scattering amplitude. However, these corrections are important to achieve a reasonable description of $E_{1+}^{3/2}$. At the same time, the description of the $I = 1/2$ channel gets worsened significantly. The overall reproduction of the s- and p-wave multipoles is worse than in the $Q^3 + \epsilon^2$ approach. However, the given estimate of the leading and subleading $\gamma N\Delta$ coupling constants b_1 and h_1 can be taken as reliable, because the isospin-3/2 channel is very well described. Also, the values agree with our findings from Ref. [1]. Notice further that while the explicit treatment of the Δ resonance in χPT helps to avoid the unnecessary lowering of the breakdown scale Λ_b, the expansion parameter in the Δ-full scheme becomes $\propto \Delta$. It is, therefore, not *a priori* clear that the framework with explicit Δ degrees of freedom features a smaller expansion parameter. For example, the $1/m_N$ expansion of the nucleon polarizabilities was found to converge considerably slower upon the explicit inclusion of the Δ resonance [69]. Thus, the most efficient scheme can only be determined upon performing explicit calculations.

Based on the conclusions of our analysis of pion photoproduction, we find that it would be very interesting to extend the analysis in the following points. In our work, we have focused on calculating the s- and p-wave multipoles, because they give by far the largest contributions to cross sections. However, in Refs. [110,111], the importance of d waves to observables was pointed out. Therefore, it would be worthwhile to extend the analysis to higher partial waves or to the analysis of observables directly. Also, further insight could be gained from extending the covariant analysis to higher orders ($Q^4 + \epsilon^3$ or ϵ^4) given the fairly slow convergence of the small scale expansion scheme. A Δ-less Q^4 calculation was already provided by Hilt *et al.* [54], but the improvement in the description was only moderate, especially in the Δ region. Since our analysis revealed significant improvement in the description of $I = 3/2$ multipole amplitudes in the Δ region, but a worse description of the $I = 1/2$ channels, the effects of the Q^4 (ϵ^4) terms in combination with the order-ϵ^3 terms would be most interesting to study. This will also allow one to draw a clearer conclusion about the efficiency of the SSE and the δ-counting schemes.

ACKNOWLEDGMENTS

We are grateful to Igor Strakovsky for providing us the recent SAID solution for pion photoproduction and to David Hornidge for providing the full set of cross-section and polarization asymmetry data from Refs. [38,39]. This work was supported in part by BMBF (Grant No. 05P18PCFP1), by DFG and NSFC through funds provided to the Sino-German CRC 110 "Symmetries and the Emergence of Structure in QCD" (NSFC Grant No. 12070131001, Project-ID 196253076 - TRR 110) and by DFG (Grant No. 426661267).

APPENDIX A: RELATING DIFFERENT SETS OF AMPLITUDES

The relation between the coefficients A_i and B_i of Eq. (11) and Eq. (14) can be found by equating the two representations:

$$\sum_{i=1}^{8} B_i V_i^{\mu} = \sum_{i=1}^{4} A_i \mathcal{M}_i^{\mu}. \tag{A1}$$

Remembering that V_4 and V_8 are not needed for real photons ($\epsilon \cdot k = 0, k^2 = 0$) and using the two relations obtained by current conservation of the matrix element (13), the coefficients A_i can be obtained from B_i as follows:

$$A_1 = \mathrm{i}(B_5 + m_N B_6), \quad A_2 = \mathrm{i}\frac{B_3}{k\cdot p + k\cdot p'},$$
$$A_3 = \mathrm{i}B_7, \quad A_4 = \frac{\mathrm{i}}{2}B_6. \tag{A2}$$

The relations between the invariant amplitudes A_i and the amplitudes $\mathcal{F}_i$ read

$$\mathcal{F}_1 = -\frac{W - m_N}{8\pi W}\sqrt{(E_p + m_N)(E_{p'} + m_N)} \times \left[A_1 + (W - m_N)A_4 - \frac{2\nu}{W - m_N}(A_3 - A_4)\right],$$
$$\mathcal{F}_2 = -\frac{W + m_N}{8\pi W}\,|\boldsymbol{q}|\sqrt{\frac{E_p - m_N}{E_{p'} + m_N}} \times \left[-A_1 + (W + m_N)A_4 - \frac{2\nu}{W + m_N}(A_3 - A_4)\right],$$
$$\mathcal{F}_3 = -\frac{W + m_N}{8\pi W}\,|\boldsymbol{q}|\sqrt{(E_p - m_N)(E_{p'} + m_N)} \times \left[\frac{W^2 - m_N^2}{W + m_N}A_2 + A_3 - A_4\right],$$

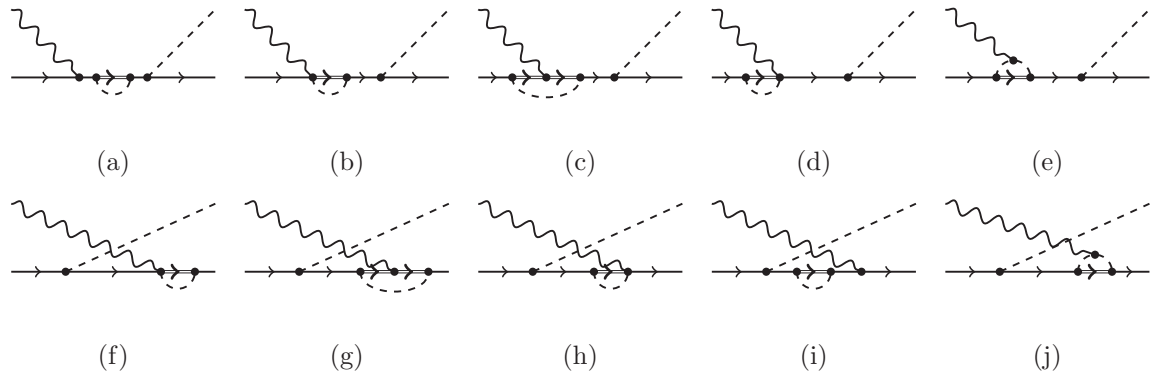

FIG. 9. First set of Δ-full loop diagrams.

$$\mathcal{F}_4 = -\frac{W-m_N}{8\pi W}|\boldsymbol{q}|^2\sqrt{\frac{E_p+m_N}{E_{p'}+m_N}} \times\left[-\frac{W^2-m_N^2}{W-m_N}A_2 + A_3 - A_4\right], \tag{A3}$$

where we have used $\nu = -\frac{1}{2}k\cdot q$ and $W=\sqrt{s}$ is the c.m. energy.

APPENDIX B: FEYNMAN DIAGRAMS

In Figs. 9–13, we present the Feynman loop diagrams for pion photoproduction that appear at order ϵ^3. We cluster them in five gauge-invariant sets. The lower-order diagrams were already shown in Ref. [1].

APPENDIX C: COUNTER TERMS

In this Appendix, we present the expressions for the renormalized quantities and the counter terms.

1. Loop integrals

The loop integral functions are defined as

$$A_0(m^2) = \frac{1}{\mathrm{i}}\int\frac{\mathrm{d}^d l}{(2\pi)^d}\frac{\mu^{4-d}}{l^2-m^2},$$

$$B_0\big(p^2,m_0^2,m_1^2\big) = \frac{1}{\mathrm{i}}\int\frac{\mathrm{d}^d l}{(2\pi)^d}\frac{\mu^{4-d}}{\big(l^2-m_0^2\big)\big((l+p)^2-m_1^2\big)},$$

$$J_0(\omega) = \frac{1}{\mathrm{i}}\int\frac{\mathrm{d}^d l}{(2\pi)^d}\frac{\mu^{4-d}}{\big(l^2-M_\pi^2\big)(v\cdot l+\omega)},$$

$$C_0\big(p^2,(p-q)^2,q^2,m_0^2,m_1^2,m_2^2\big) = \frac{1}{\mathrm{i}}\int\frac{\mathrm{d}^d l}{(2\pi)^d}\frac{\mu^{4-d}}{\big(l^2-m_0^2\big)\big((l+p)^2-m_1^2\big)\big((l+q)^2-m_2^2\big)}. \tag{C1}$$

2. Mesonic counter terms

The renormalization rules for the pion mass, field redefinition, and decay constant are given below. We remind that the parameter α is the unphysical constant from the general pion field parametrization [Eq. (23)]:

$$M^2 = M_\pi^2 + \delta M^{(4)},\quad \delta M^{(4)} = \frac{M_\pi^2}{2F_\pi^2}\big(A_0\big(M_\pi^2\big) - 4M_\pi^2\, l_3\big), \tag{C2}$$

$$Z_\pi = 1+\delta Z_\pi^{(4)},\quad \delta Z_\pi^{(4)} = \frac{1}{F_\pi^2}\big(A_0\big(M_\pi^2\big)(1-10\alpha) - 2M_\pi^2\, l_4\big), \tag{C3}$$

$$F = F_\pi + \delta F_\pi^{(4)},\quad \delta F_\pi^{(4)} = -\frac{1}{F_\pi}\big(A_0\big(M_\pi^2\big) + M_\pi^2\, l_4\big). \tag{C4}$$

3. Heavy-baryon counter terms

a. Nucleon mass and field renormalization. The HB expressions for the redefinition of the nucleon mass and field read

$$m = m_N + \delta m^{(2)} + \delta m^{(3)},\qquad \delta m^{(2)} = 4c_1 M_\pi^2,$$
$$\delta m^{(3)} = -\frac{3g_A^2 M_\pi^2}{4F_\pi^2}J_0(0), \tag{C5}$$

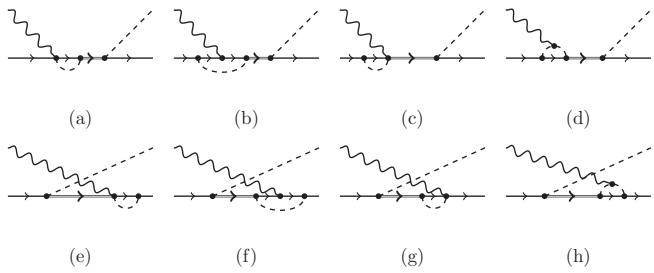

FIG. 10. Second set of Δ-full loop diagrams.

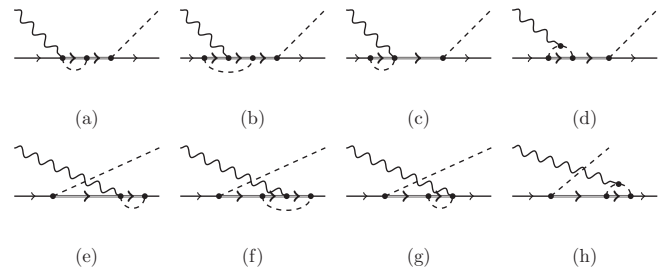

FIG. 11. Third set of Δ-full loop diagrams.

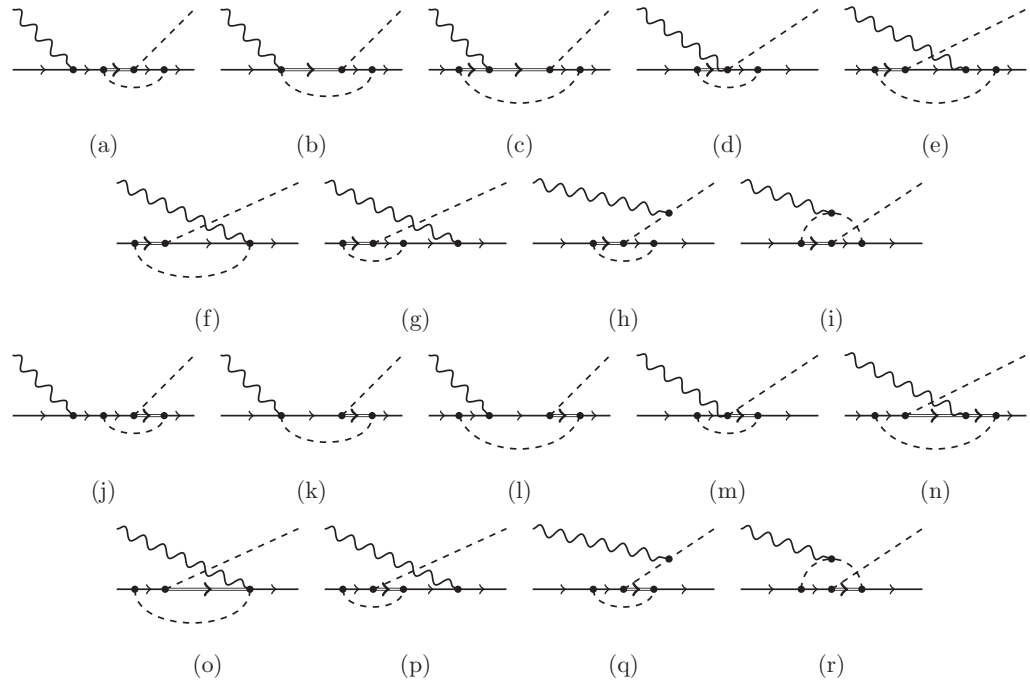

FIG. 12. Fourth set of Δ-full loop diagrams.

$$Z_N = 1 + \delta Z_N^{(3)}, \quad \delta Z_N^{(3)} = -\frac{3g_A^2 M_\pi^2}{32\pi^2 F_\pi^2} + \frac{9g_A^2}{4F_\pi^2} A_0\big(M_\pi^2\big). \tag{C6}$$

b. Δ mass and field renormalization. The Δ mass and field are renormalized as

$$\mathring{m}_\Delta = m_\Delta + \delta m_\Delta^{(2)} + \cdots, \quad \delta m_\Delta^{(2)} = 4c_1^\Delta M_\pi^2, \tag{C7}$$

and

$$Z_\Delta = 1 + \cdots, \tag{C8}$$

where the ellipses refer to terms which are not relevant at the considered order in the expansion.

c. Axial nucleon coupling. The renormalization rules for the axial nucleon coupling constant g_A in the HB sector are given below. Note that we have already taken into account the Goldberger-Treiman discrepancy to fully remove the redundant for pion photoproduction constant d_{18} from the rules. For a recent high-precision determination of the pion-nucleon coupling constants and the Goldberger-Treiman discrepancy from neutron-proton and proton-proton scattering data, see Ref. [112]. Here, g is the bare and g_A is the physical constant.

$$g = g_A + \delta g^{(3)},$$
$$\delta g^{(3)} = \left(-4d_{16} + 2d_{18} + \frac{g_A^3}{16\pi^2 F_\pi^2}\right) M_\pi^2 - \frac{\big(g_A + 2g_A^3\big)}{F_\pi^2} A_0\big(M_\pi^2\big). \tag{C9}$$

d. Electromagnetic form factors of the nucleon. The replacement rules for the counter terms of the constants c_6 and c_7 are given below, where we denote the renormalized quantities by the bar:

$$c_6 = \bar{c}_6 + \delta c_6^{(3)}, \qquad \delta c_6^{(3)} = -\frac{2m_N g_A^2}{F_\pi^2} J_0(0), \tag{C10}$$

$$c_7 = \bar{c}_7 + \delta c_7^{(3)}, \qquad \delta c_7^{(3)} = \frac{m_N g_A^2}{F_\pi^2} J_0(0). \tag{C11}$$

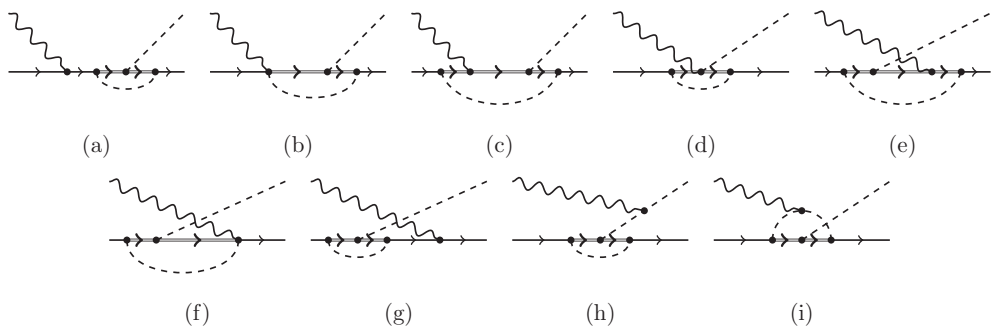

FIG. 13. Fifth set of Δ-full loop diagrams.

4. Covariant counter terms

a. Nucleon mass and field renormalization. In the following, we introduce the dimensionless parameters $\alpha = \frac{M_\pi}{m_N}$ and $\beta = \frac{m_\Delta}{m_N}$. The ratio of the masses α is not to be confused with the unphysical off-shell parameter α. The renormalization rules for the nucleon mass and field redefinition are given below. For convenience, we give the contributions arising from the Δ resonance separately. This means that all corrections $\delta x^{(i,\Delta)}$ are set to zero in the Δ-less case:

$$m = m_N + \delta m_N^{(2)} + \delta m_N^{(3)} + \delta m_N^{(3,\Delta)}, \tag{C12}$$

$$\delta m_N^{(2)} = 4M_\pi^2\, c_1, \tag{C13}$$

$$\delta m_N^{(3)} = -\frac{3g_A^2 m_N}{2F_\pi^2}\big(A_0\big(m_N^2\big) + M_\pi^2 B_0\big(m_N^2, M_\pi^2, m_N^2\big)\big), \tag{C14}$$

$$\begin{aligned}\delta m_N^{(3,\Delta)} = &-\frac{h_A^2 m_N^3}{576\,\pi^2 F_\pi^2 \beta^2}[\alpha^4(16\beta+13) - 4\alpha^2(3\beta+2) + 3\beta^4 - 12\beta^3 - 4\beta^2 + 4\beta + 2] \\ &+ \frac{m_N h_A^2}{6F_\pi^2\beta^2}\big[(\alpha^4 - \alpha^2(2\beta^2 - 6\beta - 5) + (\beta-1)(\beta+1)^3)A_0\big(M_\pi^2\big) \\ &- (\alpha^4 - 2\alpha^2(\beta^2+\beta+1) + \beta^4 + 2\beta^3 - \beta^2 + 2\beta + 1)A_0\big(m_\Delta^2\big) \\ &- (\alpha^2 - (\beta-1)^2)(\alpha^2 - (\beta+1)^2)^2 m_N^2\, B_0\big(m_N^2, M_\pi^2, m_\Delta^2\big)\big],\end{aligned} \tag{C15}$$

$$Z_N = 1 + \delta Z_N^{(3)} + \delta Z_N^{(3,\Delta)}, \tag{C16}$$

$$\delta Z_N^{(3)} = \frac{3g_A^2}{4F_\pi^2(\alpha^2-4)}\left[\frac{M_\pi^2}{4\pi^2} + (5\alpha^2 - 12)A_0\big(M_\pi^2\big) - 4\alpha^2 A_0\big(m_N^2\big) - 4M_\pi^2(\alpha^2-3)B_0\big(m_N^2, M_\pi^2, m_N^2\big)\right], \tag{C17}$$

$$\begin{aligned}\delta Z_N^{(3,\Delta)} = &\frac{h_A^2}{6F_\pi^2\beta^2}\big[(3\alpha^4 - \alpha^2(6\beta^2 + 4\beta + 9) + (\beta+1)^2(3\beta^2 - 2\beta + 5))A_0\big(M_\pi^2\big) \\ &- (3\alpha^4 + \alpha^2(-6\beta^2 - 4\beta + 2) + 3\beta^4 + 4\beta^3 + \beta^2 - 8\beta - 5)A_0\big(m_\Delta^2\big) \\ &- (3\alpha^6 - \alpha^4(9\beta^2 + 4\beta + 1) - \alpha^2(-9\beta^4 - 8\beta^3 - 2\beta^2 + 4\beta + 7) \\ &- (\beta+1)^3(3\beta^3 - 5\beta^2 + 7\beta - 5))m_N^2\, B_0\big(m_N^2, M_\pi^2, m_\Delta^2\big)\big].\end{aligned} \tag{C18}$$

b. Δ mass and field renormalization. The Δ mass and field are renormalized as

$$\mathring{m}_\Delta = m_\Delta + \delta m_\Delta^{(2)} + \cdots, \quad \delta m_\Delta^{(2)} = 4c_1^\Delta M_\pi^2, \tag{C19}$$

and

$$Z_\Delta = 1 + \cdots, \tag{C20}$$

where the ellipses refer to terms which are not relevant at the considered order in the expansion.

c. Axial nucleon coupling. The renormalization rules for the axial nucleon coupling constant g_A are given below. Note that we use the auxiliary variables a_i, b_i, and c_i only in this particular context for reasons of clarity and comprehensibility:

$$g = g_A + \delta g^{(3)} + \delta g^{(3,\Delta)}, \tag{C21}$$

$$\begin{aligned}\delta g^{(3)} = &-2(2d_{16} - d_{18})M_\pi^2 - \frac{3g_A^3 M_\pi^2}{16\pi^2 F_\pi^2(\alpha^2-4)} - \frac{g_A}{F_\pi^2(\alpha^2-4)}\big[\big(\alpha^2 - 4 + 2g_A^2(2\alpha^2-5)\big)A_0\big(M_\pi^2\big) \\ &+ \big(8 - \big(2 + 3g_A^2\big)\alpha^2\big)A_0\big(m_N^2\big) + g_A^2 m_N^2(\alpha^2-4)B_0\big(M_\pi^2, m_N^2, m_N^2\big) \\ &+ \big(8 - 2\alpha^2 - 3g_A^2(\alpha^2-3)\big)M_\pi^2\, B_0\big(m_N^2, M_\pi^2, m_N^2\big) + g_A^2 M_\pi^2 m_N^2(\alpha^2-4)C_0\big(m_N^2, M_\pi^2, m_N^2, M_\pi^2, m_N^2, m_N^2\big)\big],\end{aligned} \tag{C22}$$

$$\begin{aligned}\delta g^{(3,\Delta)} = &\, a_0 + a_1 A_0\big(M_\pi^2\big) + a_2 A_0\big(m_N^2\big) + a_3 A_0\big(m_\Delta^2\big) + b_1 B_0\big(M_\pi^2, m_N^2, m_\Delta^2\big) + b_2 B_0\big(M_\pi^2, m_\Delta^2, m_\Delta^2\big) \\ &+ b_3 B_0\big(m_N^2, M_\pi^2, m_N^2\big) + b_4 B_0\big(m_N^2, M_\pi^2, m_\Delta^2\big) + c_1 C_0\big(m_N^2, M_\pi^2, m_N^2, M_\pi^2, m_N^2, m_\Delta^2\big) \\ &+ c_2 C_0\big(m_N^2, M_\pi^2, m_N^2, M_\pi^2, m_\Delta^2, m_\Delta^2\big),\end{aligned} \tag{C23}$$

$$\begin{aligned}a_0 = &-\frac{g_A h_A^2 m_N^2}{5184\,\pi^2 F_\pi^2 \beta^2}[\alpha^4(24\beta + 325) - 4\alpha^2(3\beta^4 - 6\beta^3 - 8\beta^2 + 140\beta + 45) \\ &+ 12\alpha^6 - 69\beta^4 - 384\beta^3 + 100\beta^2 + 248\beta + 158]\end{aligned}$$

$$
\begin{aligned}
&- \frac{5g_1h_A^2m_N^2}{31104\,\pi^2F_\pi^2\beta^4}[3\alpha^{10} - \alpha^8(3\beta^2+5\beta+9) - \alpha^6(3\beta^4-10\beta^2-30\beta+60)\\
&+\alpha^4(3\beta^6+5\beta^5-3\beta^4-20\beta^3-114\beta^2-248\beta-34)\\
&-2\alpha^2(7\beta^6+59\beta^5-129\beta^4-59\beta^3-76\beta^2-68\beta-2)\\
&-2\beta(17\beta^5-82\beta^4+18\beta^3+28\beta^2+42\beta+20)], \qquad \text{(C24)}\\
a_1 = &-\frac{g_Ah_A^2}{54F_\pi^2\beta^2}[4\alpha^6+\alpha^4(-8\beta^2-8\beta+31)+\alpha^2(4\beta^4+8\beta^3-46\beta^2-69)+23\beta^4+4\beta^3+12\beta^2+56\beta+25]\\
&+\frac{5g_1h_A^2}{972F_\pi^2\beta^4}[3\alpha^{10}-\alpha^8(9\beta^2+5\beta+10)+\alpha^6(9\beta^4+10\beta^3+23\beta^2+17\beta+6)\\
&-\alpha^4(3\beta^6+5\beta^5+27\beta^4+36\beta^3+55\beta^2+33\beta-35)\\
&+2\alpha^2(7\beta^6+17\beta^5+17\beta^4-14\beta^3+44\beta^2+71\beta+21)-2(\beta+1)^2(7\beta^4-4\beta^3-9\beta^2+10\beta+2)], \qquad \text{(C25)}\\
a_2 = &\frac{2g_Ah_A^2}{27F_\pi^2\alpha^2\beta^2}[5\alpha^6+3\alpha^4(2\beta+9)+\alpha^2(-3\beta^3-6\beta^2+33\beta+16)+6(\beta-1)(\beta+1)^2], \qquad \text{(C26)}\\
a_3 = &\frac{g_Ah_A^2}{54F_\pi^2\alpha^2\beta^2}[4\alpha^8+\alpha^6(-8\beta^2-8\beta+15)+\alpha^4(4\beta^4+8\beta^3-50\beta^2-8\beta+30)\\
&+\alpha^2(23\beta^4+16\beta^3+13\beta^2-92\beta-73)-24(\beta-1)(\beta+1)^2]\\
&+\frac{5g_1h_A^2}{972F_\pi^2\beta^4}[3\alpha^{10}-\alpha^8(9\beta^2+5\beta+7)+\alpha^6(9\beta^4+10\beta^3+17\beta^2+12\beta-1)\\
&-\alpha^4(3\beta^6+5\beta^5+24\beta^4+31\beta^3+42\beta^2-15\beta-15)\\
&+2\alpha^2(7\beta^6+17\beta^5+10\beta^4-5\beta^3+18\beta^2-25\beta-7)-14\beta^6-20\beta^5+34\beta^4-20\beta^3+22\beta^2+28\beta+4], \qquad \text{(C27)}\\
b_1 = &\frac{2g_Ah_A^2m_N^2}{9F_\pi^2\alpha^2\beta^2}[\alpha^6+\alpha^4\beta(7\beta+3)+\alpha^2(-2\beta^4+\beta^3+\beta^2-5\beta-3)+2(\beta-1)^2(\beta+1)^3], \qquad \text{(C28)}\\
b_2 = &-\frac{5g_1h_A^2m_N^2}{486F_\pi^2\beta^3}[5\alpha^6+\alpha^4(8\beta^2-6\beta-11)-2\alpha^2(8\beta^4+18\beta^3+13\beta^2-6\beta-3)\\
&+4\beta^2(3\beta^4+6\beta^3-2\beta^2+6\beta+3)], \qquad \text{(C29)}\\
b_3 = &\frac{2g_Ah_A^2m_N^2}{27F_\pi^2\alpha^2\beta^2}[5\alpha^8+2\alpha^6(3\beta+7)+\alpha^4(-3\beta^3-12\beta^2+24\beta+5)\\
&+12\alpha^2(\beta-1)(\beta+1)^2-6(\beta^5-\beta^3+\beta^2-1)], \qquad \text{(C30)}\\
b_4 = &\frac{g_Ah_A^2m_N^2}{54F_\pi^2\alpha^2\beta^2}[4\alpha^{10}+\alpha^8(-12\beta^2-8\beta+11)+\alpha^6(12\beta^4+16\beta^3-61\beta^2+3)\\
&+\alpha^4(-4\beta^6-8\beta^5+73\beta^4+48\beta^3+2\beta^2-96\beta-79)-\alpha^2(\beta+1)^2(23\beta^4-30\beta^3+26\beta^2+66\beta-85)\\
&+24(\beta^5-\beta^3+\beta^2-1)]\\
&+\frac{5g_1h_A^2m_N^2}{972F_\pi^2\beta^4}[3\alpha^{12}-\alpha^{10}(12\beta^2+5\beta+10)+\alpha^8(18\beta^4+15\beta^3+30\beta^2+17\beta+6)\\
&-\alpha^6(12\beta^6+15\beta^5+44\beta^4+48\beta^3+54\beta^2-7\beta-16)\\
&+\alpha^4(3\beta^8+5\beta^7+38\beta^6+65\beta^5+76\beta^4+51\beta^3+44\beta^2-73\beta-29)\\
&-2\alpha^2(7\beta^8+17\beta^7+17\beta^6-3\beta^5-12\beta^4+23\beta^3-7\beta^2-41\beta-9)\\
&+2(\beta+1)^3(7\beta^5+\beta^4-17\beta^3+19\beta^2-8\beta-2)], \qquad \text{(C31)}\\
c_1 = &\frac{4g_Ah_A^2m_N^4}{9F_\pi^2\alpha^2\beta^2}[\alpha^8+2\alpha^6(2\beta^2+\beta-1)-2\alpha^4\beta(\beta^3+\beta+2)+2\alpha^2(\beta-1)^2(\beta+1)^3\\
&-(\beta-1)^2(\beta+1)^3(\beta^2-\beta+1)], \qquad \text{(C32)}
\end{aligned}
$$

$$c_2 = -\frac{5g_1h_A^2m_N^4}{81F_\pi^2\beta^3}[\alpha^8+\alpha^6(2\beta^2-2\beta-3)+\alpha^4(-6\beta^4-6\beta^3-7\beta^2+4\beta+3)$$
$$+\alpha^2(\beta+1)^2(5\beta^4-4\beta^3+8\beta^2-1)-2(\beta-1)^2\beta^2(\beta+1)^4]. \tag{C33}$$

d. Electromagnetic form factors of the nucleon. The renormalization rules of the two relevant LECs c_6 and c_7 are given below. We remind the reader that $\bar{c}_6$ and $\bar{c}_7$ are the renormalized quantities. Note that we use the auxiliary variables a_i, b_i, and c_i only in this particular context for reasons of clarity and comprehensibility:

$$c_6 = \bar{c}_6 + \delta c_6^{(3)} + \delta c_6^{(3,\Delta)}, \tag{C34}$$
$$\delta c_6^{(3)} = \frac{g_A^2}{(\alpha^2-4)F_\pi^2}\left[\frac{m_N^2(4-3\alpha^2)}{16\pi^2}+(20-6\alpha^2)A_0\big(M_\pi^2\big)-2(8-3\alpha^2)A_0\big(m_N^2\big)\right.$$
$$\left.+2m_N^2(8-13\alpha^2+3\alpha^4)B_0\big(m_N^2,M_\pi^2,m_N^2\big)\right], \tag{C35}$$
$$\delta c_6^{(3,\Delta)} = a_0 + a_1A_0\big(M_\pi^2\big)+a_2A_0\big(m_\Delta^2\big)+b_1B_0\big(m_N^2,M_\pi^2,m_\Delta^2\big), \tag{C36}$$
$$a_0 = -\frac{h_A^2m_N^2}{1296\pi^2F_\pi^2\beta^4}[\alpha^4(-27\beta^2+160\beta+145)+20\alpha^2(6\beta^3-7\beta^2-9\beta-4)+27\beta^6$$
$$+92\beta^5-281\beta^4-44\beta^3+75\beta^2+60\beta+20], \tag{C37}$$
$$a_1 = -\frac{2h_A^2}{81F_\pi^2\beta^4}[\alpha^4(27\beta^2+20\beta+15)+\alpha^2(-54\beta^4-40\beta^3-7\beta^2+120\beta+75)$$
$$+27\beta^6+20\beta^5-35\beta^4+6\beta^3+47\beta^2-20\beta-15], \tag{C38}$$
$$a_2 = \frac{2h_A^2}{81F_\pi^2\beta^4}[\alpha^4(27\beta^2+20\beta+15)-2\alpha^2(27\beta^4+20\beta^3-10\beta^2+20\beta+15)+27\beta^6$$
$$+20\beta^5-62\beta^4-86\beta^3-62\beta^2+20\beta+15], \tag{C39}$$
$$b_1 = \frac{2h_A^2m_N^2}{81F_\pi^2\beta^4}[\alpha^4(27\beta^2+20\beta+15)-2\alpha^2(27\beta^4-7\beta^3-30\beta^2+5\beta+15)+27\beta^6$$
$$-34\beta^5-21\beta^4+98\beta^3-57\beta^2-10\beta+15](-1+\alpha^2-2\beta-\beta^2), \tag{C40}$$
$$c_7 = \bar{c}_7 + \delta c_7^{(3)} + \delta c_7^{(3,\Delta)}, \tag{C41}$$
$$\delta c_7^{(3)} = \frac{g_A^2}{(\alpha^2-4)F_\pi^2}\left[-\frac{m_N^2}{2\pi^2}-4A_0\big(M_\pi^2\big)+8A_0\big(m_N^2\big)-4m_N^2(2-\alpha^2)B_0\big(m_N^2,M_\pi^2,m_N^2\big)\right], \tag{C42}$$
$$\delta c_7^{(3,\Delta)} = a_0 + a_1A_0\big(M_\pi^2\big)+a_2A_0\big(m_\Delta^2\big)+b_1B_0\big(m_N^2,M_\pi^2,m_\Delta^2\big), \tag{C43}$$
$$a_0 = -\frac{h_A^2m_N^2}{1296\pi^2F_\pi^2\beta^4}[\alpha^4(32\beta+29)+2\alpha^2(12\beta^3-23\beta^2-18\beta-8)+4\beta^5-67\beta^4+2\beta^3+24\beta^2+12\beta+4], \tag{C44}$$
$$a_1 = \frac{2h_A^2}{81F_\pi^2\beta^4}[\alpha^4(4\beta+3)+\alpha^2(-8\beta^3+4\beta^2+24\beta+15)+4\beta^5-7\beta^4-15\beta^3+4\beta^2-4\beta-3], \tag{C45}$$
$$a_2 = -\frac{2h_A^2}{81F_\pi^2\beta^4}[\alpha^4(4\beta+3)-2\alpha^2(4\beta^3-2\beta^2+4\beta+3)+4\beta^5-7\beta^4-\beta^3-7\beta^2+4\beta+3], \tag{C46}$$
$$b_1 = \frac{2h_A^2m_N^2}{81F_\pi^2\beta^4}(1-\alpha^2+2\beta+\beta^2)[\alpha^4(4\beta+3)-2\alpha^2(4\beta^3-6\beta^2+\beta+3)+4\beta^5-15\beta^4+25\beta^3-6\beta^2-2\beta+3]. \tag{C47}$$

e. $\pi N\Delta$ coupling. Here, we give the necessary shift of the $\pi N\Delta$ coupling h_A:

$$h = h_A + \delta h_A^{(2)}, \quad \delta h_A^{(2)} = b_3(m_N-m_\Delta)+b_6\frac{M_\pi^2+m_N^2-m_\Delta^2}{2m_N}. \tag{C48}$$

f. Electromagnetic transition form factors. Here, we give the shift for the coupling constants b_1 and h_1. Note that the auxiliary variables a_i, b_i, and c_i are used only in this particular context. Taking the real part of the corrections to b_1 and h_1 ensures that the

bare LECs are real, which is necessary for the Lagrangian to be Hermitian:

$$b_1 = \bar{b}_1 + \delta b_1^{(3)}, \tag{C49}$$

$$\begin{aligned}\delta b_1^{(3)} = \mathrm{Re}\big[&a_0 + a_1 A_0(M_\pi^2) + a_2 A_0\big(m_N^2\big) + a_3 A_0\big(m_\Delta^2\big) + b_1 B_0\big(m_N^2, M_\pi^2, m_N^2\big) + b_2 B_0\big(m_N^2, M_\pi^2, m_\Delta^2\big)\\ &+ b_3 B_0\big(m_\Delta^2, M_\pi^2, m_N^2\big) + b_4 B_0\big(m_\Delta^2, M_\pi^2, m_\Delta^2\big) + c_1 C_0\big(0, m_\Delta^2, m_N^2, M_\pi^2, M_\pi^2, m_N^2\big) + c_2 C_0\big(0, m_\Delta^2, m_N^2, M_\pi^2, M_\pi^2, m_\Delta^2\big)\\ &+ c_3 C_0(m_N^2, 0, m_\Delta^2, M_\pi^2, m_N^2, m_N^2) + c_4 C_0\big(m_N^2, 0, m_\Delta^2, M_\pi^2, m_\Delta^2, m_\Delta^2\big)\big],\end{aligned} \tag{C50}$$

$$\begin{aligned}a_0 = {}&2m_N(\beta-1)h_{15} + m_N(\beta^2-1)h_{16} - \frac{g_A h_A m_N}{16\pi^2 F_\pi^2(\beta^2-1)}[2\alpha^2+\beta^2-3\beta]\\ &+ \frac{5g_1 h_A m_N}{10368\pi^2 F_\pi^2\beta^4(\beta^2-1)}[\alpha^6(3\beta^3-2\beta^2-3\beta+2)\beta - \alpha^4(3\beta^6+3\beta^5+6\beta^4+117\beta^3+3\beta^2+8\beta+4)\\ &- \alpha^2(3\beta^8-2\beta^7+\beta^6+74\beta^5-130\beta^4-264\beta^3+36\beta^2-6) + 3\beta^{10}+3\beta^9-6\beta^8-617\beta^7-153\beta^6\\ &+ 766\beta^5-84\beta^4-82\beta^3+26\beta^2+2\beta-2],\end{aligned} \tag{C51}$$

$$\begin{aligned}a_1 = {}&\frac{g_A h_A}{F_\pi^2 m_N(\beta-1)} + \frac{5g_1 h_A}{324F_\pi^2 m_N\beta^6(\beta^2-1)}[\alpha^6\beta^3(3\beta^3-2\beta^2-3\beta+2)\\ &- \alpha^4(9\beta^8-\beta^7+\beta^6-7\beta^5-2\beta^4-2\beta^2+2) + \alpha^2\beta^2(9\beta^8+4\beta^7+5\beta^5+43\beta^4+\beta^3-8\beta^2+22\beta-4)\\ &- \beta^3(3\beta^9+3\beta^8-4\beta^7-\beta^6+32\beta^5+13\beta^4-68\beta^3+75\beta^2+25\beta-6)],\end{aligned} \tag{C52}$$

$$a_2 = \frac{g_A h_A(1-3\beta)}{F_\pi^2 m_N(\beta^2-1)}, \tag{C53}$$

$$\begin{aligned}a_3 = {}&-\frac{5g_1 h_A}{324F_\pi^2 m_N\beta^6(\beta^2-1)}[\alpha^6\beta^3(3\beta^3-2\beta^2-3\beta+2) - \alpha^4(9\beta^8-\beta^7-2\beta^6-5\beta^5+\beta^4-2\beta^3-2\beta^2+2)\\ &+ \alpha^2\beta^3(9\beta^7+4\beta^6-6\beta^5+4\beta^4+42\beta^3-82\beta^2+75\beta+26)\\ &- \beta^3(3\beta^9+3\beta^8-7\beta^7-4\beta^6+36\beta^5-62\beta^4-5\beta^3+21\beta^2+81\beta+6)],\end{aligned} \tag{C54}$$

$$b_1 = -\frac{g_A h_A m_N}{F_\pi^2(\beta^2-1)^2}[\alpha^2(\beta^3-2\beta^2-2\beta-1) + 2\beta(\beta^2-\beta+2)], \tag{C55}$$

$$\begin{aligned}b_2 = {}&-\frac{5g_1 h_A m_N}{324F_\pi^2\beta^3(\beta^2-1)^2}[\alpha^8(3\beta-2)(\beta^2-1)^2 - \alpha^6(12\beta^6-3\beta^5-14\beta^4-2\beta^3+13\beta-6)\beta\\ &+ \alpha^4(18\beta^8+3\beta^7-20\beta^6-3\beta^5+46\beta^4-47\beta^3-104\beta^2-41\beta+4)\beta\\ &+ \alpha^2(-12\beta^{11}-7\beta^{10}+22\beta^9+4\beta^8-84\beta^7-10\beta^6+152\beta^5+72\beta^4+80\beta^3+65\beta^2-2\beta+8)\\ &+ 3\beta^{13}+3\beta^{12}-10\beta^{11}-7\beta^{10}+43\beta^9+36\beta^8-172\beta^7-6\beta^6-23\beta^5+19\beta^4-46\beta^3+33\beta^2-11\beta-6],\end{aligned} \tag{C56}$$

$$b_3 = -\frac{g_A h_A m_N\beta}{F_\pi^2(\beta^2-1)^2}[\alpha^2(3\beta+1) + \beta^3 - 5\beta^2 + \beta - 1], \tag{C57}$$

$$\begin{aligned}b_4 = {}&-\frac{5g_1 h_A m_N}{162F_\pi^2\beta^6(\beta^2-1)^2}[\alpha^6(4\beta^5-3\beta^4-2\beta^2+1) + 2\alpha^4\beta^2(11\beta^5+11\beta^4+17\beta^3+4\beta^2-6\beta-1)\\ &+ 2\alpha^2\beta^4(23\beta^5-23\beta^4-62\beta^3-21\beta^2+6\beta+5) + 36(3\beta^{10}-\beta^9-\beta^8+\beta^6)],\end{aligned} \tag{C58}$$

$$c_1 = -\frac{2g_A h_A m_N^3\alpha^2(\alpha^2+\beta^2-1)}{F_\pi^2(\beta^2-1)}, \tag{C59}$$

$$c_2 = -\frac{10g_1 h_A m_N^3}{9F_\pi^2\beta(\beta^2-1)}[\alpha^6 - \alpha^4(\beta^2-\beta+1) + 3\alpha^2\beta^2(\beta^2-1)], \tag{C60}$$

$$c_3 = -\frac{2g_A h_A m_N^3\beta}{F_\pi^2(\beta^2-1)}[\alpha^2-\beta^2+\beta-2], \tag{C61}$$

$$c_4 = \frac{10g_1 h_A m_N^3}{27F_\pi^2(\beta^2-1)}[\alpha^4(\beta-4) - \alpha^2(4\beta^3-8\beta^2-\beta-4) - 3(3\beta^4-\beta^3-\beta^2+1)], \tag{C62}$$

$$h_1 = \bar{h}_1 + \delta h^{(3)}, \tag{C63}$$

$$\begin{aligned}\delta h^{(3)} &= \mathrm{Re}\big[a_0 + a_1 A_0\big(M_\pi^2\big) + a_2 A_0\big(m_N^2\big) + a_3 A_0\big(m_\Delta^2\big) + b_1 B_0\big(m_N^2, M_\pi^2, m_N^2\big) + b_2 B_0\big(m_N^2, M_\pi^2, m_\Delta^2\big)\\ &\quad + b_3 B_0\big(m_\Delta^2, M_\pi^2, m_N^2\big) + b_4 B_0\big(m_\Delta^2, M_\pi^2, m_\Delta^2\big) + c_1 C_0\big(0, m_\Delta^2, m_N^2, M_\pi^2, M_\pi^2, m_N^2\big) + c_2 C_0\big(0, m_\Delta^2, m_N^2, M_\pi^2, M_\pi^2, m_\Delta^2\big)\\ &\quad + c_3 C_0\big(m_N^2, 0, m_\Delta^2, M_\pi^2, m_N^2, m_N^2\big) + c_4 C_0\big(m_N^2, 0, m_\Delta^2, M_\pi^2, m_\Delta^2, m_\Delta^2\big)\big], \qquad \text{(C64)}\\ a_0 &= 2m_N h_{15} - \frac{g_A h_A m_N(\alpha^2-\beta)}{4\pi^2 F_\pi^2(\beta-1)^2(\beta+1)}\\ &\quad + \frac{5g_1 h_A m_N}{10368\pi^2 F_\pi^2 \beta^4(\beta-1)^2(\beta+1)}[3\alpha^6(\beta-1)^2(\beta+1)\beta - \alpha^4(3\beta^6+2\beta^5+7\beta^4+275\beta^3+2\beta^2-5\beta+4)\\ &\quad - \alpha^2(3\beta^8-3\beta^7+\beta^6-45\beta^5-222\beta^4-376\beta^3+56\beta^2+16\beta-6)\\ &\quad + 3\beta^{10}+2\beta^9-5\beta^8-587\beta^7+74\beta^6+717\beta^5-386\beta^4-138\beta^3+28\beta^2+6\beta-2], \qquad \text{(C65)}\\ a_1 &= \frac{2g_A h_A}{F_\pi^2 m_N(\beta-1)^2} + \frac{5g_1 h_A}{324F_\pi^2 m_N \beta^6(\beta-1)^2(\beta+1)}[3\alpha^6(\beta-1)^2\beta^3(\beta+1)\\ &\quad - \alpha^4(9\beta^8-4\beta^7+2\beta^6-12\beta^5-3\beta^4+10\beta^3-2\beta^2-2\beta+2)\\ &\quad + \alpha^2\beta^2(9\beta^8+\beta^7+2\beta^6+\beta^5+48\beta^4+36\beta^3+45\beta^2+30\beta-28)\\ &\quad - \beta^3(3\beta^9+2\beta^8-3\beta^7+\beta^6+35\beta^5+83\beta^4-51\beta^3+37\beta^2+40\beta-3)], \qquad \text{(C66)}\\ a_2 &= -\frac{4g_A h_A \beta}{F_\pi^2 m_N(\beta-1^2)(\beta+1)}, \qquad \text{(C67)}\\ a_3 &= -\frac{5g_1 h_A}{324F_\pi^2 m_N \beta^6(\beta-1)^2(\beta+1)}[3\alpha^6(\beta-1)^2\beta^3(\beta+1) - \alpha^4(9\beta^8-4\beta^7-\beta^6-9\beta^5+7\beta^3-2\beta^2-2\beta+2)\\ &\quad + \alpha^2\beta^2(9\beta^8+\beta^7-4\beta^6+2\beta^5+46\beta^4-44\beta^3+129\beta^2+29\beta-24)\\ &\quad - \beta^3(3\beta^9+2\beta^8-6\beta^7-\beta^6+38\beta^5+132\beta^4+\beta^3-136\beta^2+108\beta+3)], \qquad \text{(C68)}\\ b_1 &= -\frac{2g_A h_A m_N}{F_\pi^2(\beta-1)^3(\beta+1)^2}[\alpha^2(\beta^3-2\beta^2-2\beta-1)+\beta(\beta^2+3)], \qquad \text{(C69)}\\ b_2 &= -\frac{5g_1 h_A m_N}{324F_\pi^2\beta^3(\beta-1)^3(\beta+1)^2}[3\alpha^8(\beta-1)^3(\beta+1)^2 - \alpha^6(12\beta^6-7\beta^5-13\beta^4-2\beta^3-2\beta^2+17\beta-5)\beta\\ &\quad + \alpha^4(18\beta^9-3\beta^8-17\beta^7-5\beta^6+47\beta^5-115\beta^4-143\beta^3-79\beta^2+3\beta+6)\\ &\quad - \alpha^2(12\beta^{10}+3\beta^9-19\beta^8+88\beta^6-70\beta^5-262\beta^4-120\beta^3-80\beta^2-125\beta-3)\beta\\ &\quad + 3\beta^{13}+2\beta^{12}-9\beta^{11}-3\beta^{10}+44\beta^9+5\beta^8-262\beta^7-98\beta^6+15\beta^5+84\beta^4-65\beta^3+13\beta^2-14\beta-3], \qquad \text{(C70)}\\ b_3 &= -\frac{2g_A h_A m_N \beta}{F_\pi^2(\beta-1)^3(\beta+1)^2}[\alpha^2(3\beta+1)-3\beta^2-1], \qquad \text{(C71)}\\ b_4 &= \frac{5g_1 h_A m_N}{162F_\pi^2\beta^6(\beta-1)^3(\beta+1)^2}[\alpha^6(\beta^5+3\beta^4-6\beta^3+2\beta^2+\beta-1)\\ &\quad - 2\alpha^4\beta^2(43\beta^5+33\beta^4+13\beta^3-15\beta^2-7\beta+5)\\ &\quad + 2\alpha^2\beta^4(23\beta^5+69\beta^4+43\beta^3-4\beta^2+12\beta+1) - 12\beta^6(2\beta^5+13\beta^4-4\beta^2-2\beta+3)], \qquad \text{(C72)}\\ c_1 &= -\frac{2g_A h_A m_N^3 \alpha^3(2\alpha^2+\beta^2-1)}{F_\pi^2(\beta-1)^2(\beta+1)}, \qquad \text{(C73)}\\ c_2 &= -\frac{10g_1 h_A m_N^3 \alpha^2}{9F_\pi^2\beta(\beta-1)^2(\beta+1)}[2\alpha^4+\alpha^2(-\beta^2+\beta-2)+\beta(2\beta^3-\beta^2-2\beta+1)], \qquad \text{(C74)}\\ c_3 &= -\frac{2g_A h_A m_N^3}{F_\pi^2(\beta-1)^2(\beta+1)}[\alpha^2(\beta+1)-\beta(\beta^2+3)], \qquad \text{(C75)}\\ c_4 &= -\frac{10g_1 h_A m_N^3}{27F_\pi^2(\beta-1)^2(\beta+1)}[2\alpha^4(\beta+2)-\alpha^2(4\beta^3+11\beta^2-\beta+4)+2\beta^5+13\beta^4-4\beta^2-2\beta+3]. \qquad \text{(C76)}\end{aligned}$$

[1] J. Rijneveen, N. Rijneveen, H. Krebs, A. M. Gasparyan, and E. Epelbaum, Radiative pion photoproduction in covariant chiral perturbation theory, Phys. Rev. C **103**, 045203 (2021).

[2] S. Pastore, L. Girlanda, R. Schiavilla, M. Viviani, and R. B. Wiringa, Electromagnetic currents and magnetic moments in (χEFT), Phys. Rev. C **80**, 034004 (2009).

[3] S. Kölling, E. Epelbaum, H. Krebs, and U.-G. Meißner, Two-nucleon electromagnetic current in chiral effective field theory: One-pion exchange and short-range contributions, Phys. Rev. C **84**, 054008 (2011).

[4] S. Kölling, E. Epelbaum, and D. R. Phillips, The magnetic form factor of the deuteron in chiral effective field theory, Phys. Rev. C **86**, 047001 (2012).

[5] M. Piarulli, L. Girlanda, L. E. Marcucci, S. Pastore, R. Schiavilla, and M. Viviani, Electromagnetic structure of $A = 2$ and 3 nuclei in chiral effective field theory, Phys. Rev. C **87**, 014006 (2013).

[6] R. Schiavilla, A. Baroni, S. Pastore, M. Piarulli, L. Girlanda *et al.*, Local chiral interactions and magnetic structure of few-nucleon systems, Phys. Rev. C **99**, 034005 (2019).

[7] H. Krebs, E. Epelbaum, and U.-G. Meißner, Nuclear electromagnetic currents to fourth order in chiral effective field theory, Few-Body Syst. **60**, 31 (2019).

[8] N. M. Kroll, A Theorem on photomeson production near threshold and the suppression of pairs in pseudoscalar meson theory, Phys. Rev. **93**, 233 (1954).

[9] P. De Baenst, An improvement on the Kroll-Ruderman theorem, Nucl. Phys. B **24**, 633 (1970).

[10] A. I. Vainshtein and V. I. Zakharov, Low-energy theorems for photoproduction and electropion production at threshold, Nucl. Phys. B **36**, 589 (1972).

[11] Y. Nambu, Axial Vector Current Conservation in Weak Interactions, Phys. Rev. Lett. **4**, 380 (1960).

[12] J. Bernstein, M. Gell-Mann, and L. Michel, On the renormalization of the axial vector coupling constant in β-decay, Nuovo Cimento **16**, 560 (1960).

[13] M. Gell-Mann and M. Levy, The axial vector current in beta decay, Nuovo Cimento **16**, 705 (1960).

[14] S. L. Adler and R. F. Dashen, *Current Algebras and Applications to Particle Physics* (Benjamin, New York, 1968).

[15] S. Treiman, R. Jackiw, and D. J. Gross, *Lectures on Current Algebra and Its Applications* (Princeton University Press, Princeton, NJ, 1972).

[16] V. de Alfaro, S. Fubini, G. Furlan, and C. Rossetti, *Currents in Hadron Physics* (North-Holland, Amsterdam, 1973).

[17] E. Mazzucato, P. Argan, G. Audit, A. Bloch, N. de Botton *et al.*, Precise Measurement of Neutral-Pion Photoproduction on the Proton Near Threshold, Phys. Rev. Lett. **57**, 3144 (1986).

[18] R. Beck, F. Kalleicher, B. Schoch, J. Vogt, G. Koch, H. Stroher, V. Metag, J. C. McGeorge, J. D. Kellie, and S. J. Hall, Measurement of the $p(\gamma, \pi^0)$ Cross Section at Threshold, Phys. Rev. Lett. **65**, 1841 (1990).

[19] V. Bernard, N. Kaiser, J. Gasser, and U.-G. Meißner, Neutral pion photoproduction at threshold, Phys. Lett. B **268**, 291 (1991).

[20] V. Bernard, N. Kaiser, and U.-G. Meißner, Threshold pion photoproduction in chiral perturbation theory, Nucl. Phys. B **383**, 442 (1992).

[21] T. P. Welch *et al.*, Electroproduction of π^0 on the Proton near Threshold, Phys. Rev. Lett. **69**, 2761 (1992).

[22] H. B. van den Brink *et al.*, Neutral Pion Electroproduction on the Proton near Threshold, Phys. Rev. Lett. **74**, 3561 (1995).

[23] K. I. Blomqvist *et al.*, Precise pion electroproduction in the $p(e, e'\pi^+)n$ reaction at W = 1125 MeV, Z. Phys. A: Hadrons Nucl. **353**, 415 (1996).

[24] M. Fuchs *et al.*, Neutral pion photoproduction from the proton near threshold, Phys. Lett. B **368**, 20 (1996).

[25] J. C. Bergstrom, J. M. Vogt, R. Igarashi, K. J. Keeter, E. L. Hallin, G. A. Retzlaff, D. M. Skopik, and E. C. Booth, Measurement of the ^{1}H(γ, π^0) cross section near threshold, Phys. Rev. C **53**, R1052 (1996).

[26] J. C. Bergstrom, R. Igarashi, and J. M. Vogt, Measurement of the ^{1}H(γ, π^0) cross section near threshold. II: Pion angular distributions, Phys. Rev. C **55**, 2016 (1997).

[27] A. M. Bernstein, E. Shuster, R. Beck, M. Fuchs, B. Krusche, H. Merkel, and H. Stroher, Observation of a unitary cusp in the threshold $\gamma p \to \pi^0 p$ reaction, Phys. Rev. C **55**, 1509 (1997).

[28] M. A. Kovash (E643 Collaboration), Total cross-sections for $\pi^- p \to \gamma n$ at 10-MeV to 20-MeV, PiN Newslett. **12N3**, 51 (1997).

[29] M. O. Distler *et al.*, Measurement of Separated Structure Functions in the $p(e, e'p)\pi^0$ Reaction at Threshold and Chiral Perturbation Theory, Phys. Rev. Lett. **80**, 2294 (1998).

[30] A. Liesenfeld *et al.*, A Measurement of the axial form-factor of the nucleon by the $p(e, e'\pi^+)n$ reaction at W = 1125 MeV, Phys. Lett. B **468**, 20 (1999).

[31] E. Korkmaz *et al.*, Measurement of the $\gamma p \to \pi^+ n$ Reaction near Threshold, Phys. Rev. Lett. **83**, 3609 (1999).

[32] A. Schmidt *et al.*, Test of Low-Energy Theorems for $^1H(\overrightarrow{\gamma}, \pi^0)^1H$ in the Threshold Region, Phys. Rev. Lett. **87**, 232501 (2001); **110**, 039903(E) (2013).

[33] H. Merkel, P. Bartsch, D. Baumann, J. Bermuth, A. M. Bernstein, K. Bohinc, R. Bohm, N. Clawiter, S. Derber, M. Ding, M. O. Distler, I. Ewald, J. M. Friedrich, J. Friedrich, P. Jennewein, M. Kahrau, M. Kohl, K. W. Krygier, M. Kuss, A. Liesenfeld *et al.*, Neutral Pion Threshold Production at $Q^2 = 0.05$ GeV$^2/c^2$ and Chiral Perturbation Theory, Phys. Rev. Lett. **88**, 012301 (2001).

[34] D. Baumann, π^+-Elektroproduktion an der Schwelle, Ph.D. thesis, Johannes Gutenberg-Universität Mainz, 2005.

[35] M. Weis *et al.*, Separated cross-sections in π^0 electroproduction at threshold at $Q^2 = 0.05$ GeV$^2/c^2$, Eur. Phys. J. A **38**, 27 (2008).

[36] H. Merkel, Experimental results from MAMI, PoS **CD09**, 112 (2009).

[37] H. Merkel, P. Achenbach, C. Ayerbe Gayoso, M. Ases Antelo, D. Baumann *et al.*, Consistent threshold π^0 electro-production at $Q^2 = 0.05$, 0.10, and 0.15 GeV^2/c^2, arXiv:1109.5075.

[38] D. Hornidge *et al.*, Accurate Test of Chiral Dynamics in the $\gamma p \to \pi^0 p$ Reaction, Phys. Rev. Lett. **111**, 062004 (2013).

[39] D. Hornidge, Asymmetries for neutral pion photoproduction in the threshold region, PoS **172**, 070 (2013).

[40] R. Lindgren, K. Chirapatimol, and L. C. Smith, Precision measurements of neutral pion electroproduction near threshold: A test of chiral QCD dynamics, PoS **172**, 073 (2013).

[41] V. Bernard, N. Kaiser, J. Kambor, and U.-G. Meißner, Chiral structure of the nucleon, Nucl. Phys. B **388**, 315 (1992).

[42] V. Bernard, N. Kaiser, and U.-G. Meißner, Determining the Axial Radius of the Nucleon from Data on Pion Electroproduction, Phys. Rev. Lett. **69**, 1877 (1992).

[43] V. Bernard, N. Kaiser, T. S. H. Lee, and U.-G. Meißner, Threshold pion electroproduction in chiral perturbation theory, Phys. Rep. **246**, 315 (1994).

[44] V. Bernard, N. Kaiser, and U.-G. Meißner, Novel Pion Electroproduction Low-Energy Theorems, Phys. Rev. Lett. **74**, 3752 (1995).

[45] V. Bernard, N. Kaiser, and U.-G. Meißner, Threshold neutral pion electroproduction in heavy baryon chiral perturbation theory, Nucl. Phys. A **607**, 379 (1996); **633**, 695(E) (1998).

[46] V. Bernard, N. Kaiser, and U.-G. Meißner, Neutral pion photoproduction off nucleons revisited, Z. Phys. C **70**, 483 (1996).

[47] V. Bernard, N. Kaiser, and U.-G. Meißner, Chiral corrections to the Kroll-Ruderman theorem, Phys. Lett. B **383**, 116 (1996).

[48] V. Bernard, N. Kaiser, and U.-G. Meißner, Chiral symmetry and the reaction $\gamma p \to \pi^0 p$, Phys. Lett. B **378**, 337 (1996).

[49] H. W. Fearing, T. R. Hemmert, R. Lewis, and C. Unkmeir, Radiative pion capture by a nucleon, Phys. Rev. C **62**, 054006 (2000).

[50] A. Gasparyan and M. F. M. Lutz, Photon- and pion-nucleon interactions in a unitary and causal effective field theory based on the chiral Lagrangian, Nucl. Phys. A **848**, 126 (2010).

[51] T. Becher and H. Leutwyler, Baryon chiral perturbation theory in manifestly Lorentz invariant form, Eur. Phys. J. C **9**, 643 (1999).

[52] T. Fuchs, J. Gegelia, G. Japaridze, and S. Scherer, Renormalization of relativistic baryon chiral perturbation theory and power counting, Phys. Rev. D **68**, 056005 (2003).

[53] V. Bernard, B. Kubis, and U.-G. Meißner, The Fubini-Furlan-Rosetti sum rule and related aspects in light of covariant baryon chiral perturbation theory, Eur. Phys. J. A **25**, 419 (2005).

[54] M. Hilt, B. C. Lehnhart, S. Scherer, and L. Tiator, Pion photo- and electroproduction in relativistic baryon chiral perturbation theory and the chiral MAID interface, Phys. Rev. C **88**, 055207 (2013).

[55] M. Hilt, S. Scherer, and L. Tiator, Threshold π^0 photoproduction in relativistic chiral perturbation theory, Phys. Rev. C **87**, 045204 (2013).

[56] T. R. Hemmert, B. R. Holstein, and J. Kambor, Systematic 1/M expansion for spin 3/2 particles in baryon chiral perturbation theory, Phys. Lett. B **395**, 89 (1997).

[57] T. R. Hemmert, B. R. Holstein, and J. Kambor, Heavy baryon chiral perturbation theory with light deltas, J. Phys. G: Nucl. Part. Phys. **24**, 1831 (1998).

[58] L. W. Cawthorne and J. A. McGovern, Impact of the Delta (1232) resonance on neutral pion photoproduction in chiral perturbation theory, PoS **253**, 072 (2016).

[59] A. N. Hiller Blin, T. Ledwig, and M. J. Vicente Vacas, Chiral dynamics in the $\boldsymbol{\gamma} p \to p\pi^0$ reaction, Phys. Lett. B **747**, 217 (2015).

[60] A. N. Hiller Blin, T. Ledwig, and M. J. Vicente Vacas, $\Delta(1232)$ resonance in the $\boldsymbol{\gamma} p \to p\pi^0$ reaction at threshold, Phys. Rev. D **93**, 094018 (2016).

[61] G. H. Guerrero Navarro, M. J. Vicente Vacas, A. N. Hiller Blin, and D.-L. Yao, Pion photoproduction off nucleons in covariant chiral perturbation theory, Phys. Rev. D **100**, 094021 (2019).

[62] G. H. Guerrero Navarro and M. J. Vicente Vacas, Threshold pion electro- and photoproduction off nucleons in covariant chiral perturbation theory, Phys. Rev. D **102**, 113016 (2020).

[63] V. Pascalutsa and D. R. Phillips, Effective theory of the $\Delta(1232)$ in Compton scattering off the nucleon, Phys. Rev. C **67**, 055202 (2003).

[64] R. J. Furnstahl, N. Klco, D. R. Phillips, and S. Wesolowski, Quantifying truncation errors in effective field theory, Phys. Rev. C **92**, 024005 (2015).

[65] J. A. Melendez, S. Wesolowski, and R. J. Furnstahl, Bayesian truncation errors in chiral effective field theory: Nucleon-nucleon observables, Phys. Rev. C **96**, 024003 (2017).

[66] E. Epelbaum *et al.*, Towards high-order calculations of three-nucleon scattering in chiral effective field theory, Eur. Phys. J. A **56**, 92 (2020).

[67] D. Siemens, V. Bernard, E. Epelbaum, A. Gasparyan, H. Krebs, and U.-G. Meißner, Elastic pion-nucleon scattering in chiral perturbation theory: A fresh look, Phys. Rev. C **94**, 014620 (2016).

[68] D. Siemens, J. Ruiz de Elvira, E. Epelbaum, M. Hoferichter, H. Krebs, B. Kubis, and U.-G. Meißner, Reconciling threshold and subthreshold expansions for pion-nucleon scattering, Phys. Lett. B **770**, 27 (2017).

[69] M. Thürmann, E. Epelbaum, A. M. Gasparyan, and H. Krebs, Nucleon polarizabilities in covariant baryon chiral perturbation theory with explicit Δ degrees of freedom, Phys. Rev. C **103**, 035201 (2021).

[70] D. Hornidge (private communication).

[71] J. S. Ball, Application of the Mandelstam representation to photoproduction of pions from nucleons, Phys. Rev. **124**, 2014 (1961).

[72] G. F. Chew, M. L. Goldberger, F. E. Low, and Y. Nambu, Relativistic dispersion relation approach to photomeson production, Phys. Rev. **106**, 1345 (1957).

[73] J. Gasser and H. Leutwyler, Chiral perturbation theory to one loop, Ann. Phys. **158**, 142 (1984).

[74] N. Fettes, U.-G. Meißner, M. Mojzis, and S. Steininger, The chiral effective pion nucleon Lagrangian of order p^4, Ann. Phys. **283**, 273 (2000); **288**, 249(E) (2001).

[75] E. Epelbaum, H.-W. Hammer, and U.-G. Meißner, Modern theory of nuclear forces, Rev. Mod. Phys. **81**, 1773 (2009).

[76] T. R. Hemmert, Heavy baryon chiral perturbation theory with light deltas, Ph.D. thesis, University of Massachusetts Amherst, 1999.

[77] C. Zöller, Effective chiral nucleon-delta Lagrangian at order Q^3, Master's thesis, Ruhr-Universität Bochum, 2014.

[78] H. Krebs, E. Epelbaum, and U.-G. Meißner, Redundancy of the off-shell parameters in chiral effective field theory with explicit spin-3/2 degrees of freedom, Phys. Lett. B **683**, 222 (2010).

[79] V. Bernard, T. R. Hemmert, and U.-G. Meißner, Infrared regularization with spin 3/2 fields, Phys. Lett. B **565**, 137 (2003).

[80] S. Weinberg, Effective chiral Lagrangians for nucleon-pion interactions and nuclear forces, Nucl. Phys. B **363**, 3 (1991).

[81] V. Pascalutsa and M. Vanderhaeghen, Chiral effective-field theory in the $\Delta(1232)$ region: I. Pion electroproduction on the nucleon, Phys. Rev. D **73**, 034003 (2006).

[82] A. Denner, S. Dittmaier, M. Roth, and D. Wackeroth, Predictions for all processes $e^+e^- \to 4$ fermions $+\gamma$, Nucl. Phys. B **560**, 33 (1999).

[83] A. Denner, S. Dittmaier, M. Roth, and L. H. Wieders, Electroweak corrections to charged-current $e^+e^- \to 4$ fermion processes: Technical details and further results, Nucl. Phys. B **724**, 247 (2005); **854**, 504(E) (2012).

[84] A. Denner and S. Dittmaier, The complex-mass scheme for perturbative calculations with unstable particles, Nucl. Phys. B: Proc. Suppl. **160**, 22 (2006).

[85] D.-L. Yao, D. Siemens, V. Bernard, E. Epelbaum, A. M. Gasparyan, J. Gegelia, H. Krebs, and U.-G. Meißner, Pion-nucleon scattering in covariant baryon chiral perturbation theory with explicit Delta resonances, J. High Energ. Phys. 05 (2016) 038.

[86] J. Gasser, M. A. Ivanov, E. Lipartia, M. Mojzis, and A. Rusetsky, Ground state energy of pionic hydrogen to one loop, Eur. Phys. J. C **26**, 13 (2002).

[87] Wolfram Mathematica, https://www.wolfram.com/mathematica/.

[88] J. Kuipers, T. Ueda, J. A. M. Vermaseren, and J. Vollinga, FORM version 4.0, Comput. Phys. Commun. **184**, 1453 (2013).

[89] T. Hahn and M. Pérez-Victoria, Automated one-loop calculations in four and D dimensions, Comput. Phys. Commun. **118**, 153 (1999).

[90] H. H. Patel, Package-X: A Mathematica package for the analytic calculation of one-loop integrals, Comput. Phys. Commun. **197**, 276 (2015).

[91] P. A. Zyla *et al.*, Review of particle physics, PTEP **2020**, 083C01 (2020).

[92] V. Baru, C. Hanhart, M. Hoferichter, B. Kubis, A. Nogga, and D. R. Phillips, Precision calculation of the $\pi^- d$ scattering length and its impact on threshold πN scattering, Phys. Lett. B **694**, 473 (2011).

[93] V. Bernard, E. Epelbaum, H. Krebs, and U.-G. Meißner, New insights into the spin structure of the nucleon, Phys. Rev. D **87**, 054032 (2013).

[94] T. Appelquist and J. Carazzone, Infrared singularities and massive fields, Phys. Rev. D **11**, 2856 (1975).

[95] D. Drechsel, S. S. Kamalov, and L. Tiator, Unitary isobar model - MAID2007, Eur. Phys. J. A **34**, 69 (2007).

[96] K. M. Watson, Some general relations between the photoproduction and scattering of π mesons, Phys. Rev. **95**, 228 (1954).

[97] N. Fettes, U.-G. Meißner, and S. Steininger, Pion-nucleon scattering in chiral perturbation theory. 1. Isospin symmetric case, Nucl. Phys. A **640**, 199 (1998).

[98] C. Fernández-Ramírez and A. M. Bernstein, Upper energy limit of heavy baryon chiral perturbation theory in neutral pion photoproduction, Phys. Lett. B **724**, 253 (2013).

[99] W. J. Briscoe *et al.*, Cross section for $\gamma n \to \pi^0 n$ at the Mainz A2 experiment, Phys. Rev. C **100**, 065205 (2019).

[100] I. Strakovsky (private communication).

[101] R. L. Workman, M. W. Paris, W. J. Briscoe, and I. I. Strakovsky, Unified Chew-Mandelstam SAID analysis of pion photoproduction data, Phys. Rev. C **86**, 015202 (2012).

[102] J. A. McGovern, D. R. Phillips, and H. W. Grießhammer, Compton scattering from the proton in an effective field theory with explicit Delta degrees of freedom, Eur. Phys. J. A **49**, 12 (2013).

[103] E. Epelbaum, H. Krebs, and U.-G. Meißner, Improved chiral nucleon-nucleon potential up to next-to-next-to-next-to-leading order, Eur. Phys. J. A **51**, 53 (2015).

[104] E. Epelbaum, High-precision nuclear forces: Where do we stand? PoS **317**, 006 (2019).

[105] S. Wesolowski, R. J. Furnstahl, J. A. Melendez, and D. R. Phillips, Exploring Bayesian parameter estimation for chiral effective field theory using nucleon-nucleon phase shifts, J. Phys. G: Nucl. Part. Phys. **46**, 045102 (2019).

[106] H. Krebs, Nuclear currents in chiral effective field theory, Eur. Phys. J. A **56**, 234 (2020).

[107] S. Kölling, E. Epelbaum, H. Krebs, and U.-G. Meißner, Two-pion exchange electromagnetic current in chiral effective field theory using the method of unitary transformation, Phys. Rev. C **80**, 045502 (2009).

[108] A. A. Filin, V. Baru, E. Epelbaum, H. Krebs, D. Möller, and P. Reinert, Extraction of the Neutron Charge Radius from a Precision Calculation of the Deuteron Structure Radius, Phys. Rev. Lett. **124**, 082501 (2020).

[109] A. A. Filin, D. Möller, V. Baru, E. Epelbaum, H. Krebs, and P. Reinert, High-accuracy calculation of the deuteron charge and quadrupole form factors in chiral effective field theory, Phys. Rev. C **103**, 024313 (2021).

[110] C. Fernández-Ramírez, A. M. Bernstein, and T. W. Donnelly, The unexpected impact of D waves in low-energy neutral pion photoproduction from the proton and the extraction of multipoles, Phys. Rev. C **80**, 065201 (2009).

[111] C. Fernández-Ramírez, A. M. Bernstein, and T. W. Donnelly, Low-energy D-wave effects in neutral pion photoproduction, Phys. Lett. B **679**, 41 (2009).

[112] P. Reinert, H. Krebs, and E. Epelbaum, Precision Determination of Pion-Nucleon Coupling Constants Using Effective Field Theory, Phys. Rev. Lett. **126**, 092501 (2021).